

TDP-43 gains function due to perturbed autoregulation in a *Tardbp* knock-in mouse model of ALS-FTD

Matthew A. White^{1,2,14}, Eosu Kim^{3,4}, Amanda Duffy⁵, Robert Adalbert⁶, Benjamin U. Phillips³, Owen M. Peters^{7,15}, Jodie Stephenson^{8,16}, Sujeong Yang⁶, Francesca Massenzio^{1,2}, Ziqiang Lin^{1,2}, Simon Andrews¹, Anne Segonds-Pichon¹, Jake Metterville⁹, Lisa M. Saksida^{3,10,11}, Richard Mead⁸, Richard R. Ribchester¹², Youssef Barhomi¹³, Thomas Serre¹³, Michael P. Coleman^{1,6}, Justin Fallon⁵, Timothy J. Bussey^{3,10,11}, Robert H. Brown Jr⁹ and Jemeen Sreedharan^{1,2,14*}

Amyotrophic lateral sclerosis–frontotemporal dementia (ALS-FTD) constitutes a devastating disease spectrum characterized by 43-kDa TAR DNA-binding protein (TDP-43) pathology. Understanding how TDP-43 contributes to neurodegeneration will help direct therapeutic efforts. Here we have created a TDP-43 knock-in mouse with a human-equivalent mutation in the endogenous mouse *Tardbp* gene. TDP-43^{Q331K} mice demonstrate cognitive dysfunction and a paucity of parvalbumin interneurons. Critically, TDP-43 autoregulation is perturbed, leading to a gain of TDP-43 function and altered splicing of *Mapt*, another pivotal dementia-associated gene. Furthermore, a new approach to stratify transcriptomic data by phenotype in differentially affected mutant mice revealed 471 changes linked with improved behavior. These changes included downregulation of two known modifiers of neurodegeneration, *Atxn2* and *Arid4a*, and upregulation of myelination and translation genes. With one base change in murine *Tardbp*, this study identifies TDP-43 misregulation as a pathogenic mechanism that may underpin ALS-FTD and exploits phenotypic heterogeneity to yield candidate suppressors of neurodegenerative disease.

Amyotrophic lateral sclerosis (ALS) and frontotemporal dementia (FTD) are destructive neurodegenerative diseases that exist on a clinicopathological spectrum (ALS-FTD)¹. ALS is characterized by motor impairment and FTD by executive dysfunction, language impairment and behavioral changes. Nearly all cases of ALS, half of FTD cases, and most hereditary forms of ALS and FTD are characterized by cytoplasmic mislocalization and aggregation of TDP-43^{2,3}. The identification of mutations in the gene encoding TDP-43 (*TARDBP*) as a cause of ALS and FTD confirmed that TDP-43 plays a mechanistic role in neurodegeneration^{4,5}. This role remains undefined.

TDP-43 is a conserved RNA-binding protein with critical roles in splicing in the nervous system⁶. TDP-43 also demonstrates tight autoregulation by binding to its transcript, triggering alternative splicing of intron 7 in the *TARDBP* 3' untranslated region (UTR) and destruction of its mRNA⁷. Experimentally increasing and decreasing TDP-43 levels both cause neuronal loss, but whether human neurodegeneration is caused by a gain or loss of TDP-43

function remains unclear. Modeling of mutant TDP-43 in vivo has relied on variable degrees of transgenic overexpression of TDP-43 to replicate pathological changes seen in postmortem human tissues⁸. However, TDP-43 transgenic mouse models have demonstrated that TDP-43 aggregation is not necessary to cause neurodegeneration⁹, and whether TDP-43 aggregation is causally linked to disease onset is unclear.

A caveat of transgenic TDP-43 mouse models is that phenotypes may partly be artifacts of overexpression. Furthermore, the cell-type-specific expression of single TDP-43 splice forms in transgenic models using neuronal promoters and temporally triggered expression of transgenes in adulthood do not reflect the ubiquitous expression and alternative splicing of *Tardbp*, including that occurring during embryonic development¹⁰. To unravel the role of mutant TDP-43 in the disease pathogenesis, we created a knock-in mouse harboring only a human-equivalent point mutation in the endogenous mouse *Tardbp* gene. This model replicates the human mutant state as closely as possible, retaining the endogenous gene structure

¹The Babraham Institute, Cambridge, UK. ²Maurice Wohl Clinical Neuroscience Institute, Institute of Psychiatry, Psychology and Neuroscience, King's College London, London, UK. ³Department of Psychology and MRC/Wellcome Trust Behavioural and Clinical Neuroscience Institute, University of Cambridge, Cambridge, UK. ⁴Department of Psychiatry, Institute of Behavioral Science in Medicine, Brain Korea 21 Plus Project for Medical Sciences, Yonsei University College of Medicine, Seoul, Republic of Korea. ⁵Department of Neuroscience, Brown University, Providence, RI, USA. ⁶John van Geest Centre for Brain Repair, University of Cambridge, Cambridge, UK. ⁷The Vollum Institute, Oregon Health & Science University, Portland, OR, USA. ⁸Sheffield Institute for Translational Neuroscience, University of Sheffield, Sheffield, UK. ⁹Department of Neurology, UMass Medical School, Worcester, MA, USA. ¹⁰Molecular Medicine Research Group, Robarts Research Institute & Department of Physiology and Pharmacology, Schulich School of Medicine & Dentistry, Western University, London, ON, Canada. ¹¹The Brain and Mind Institute, Western University, London, ON, Canada. ¹²SBMS, University of Edinburgh, Edinburgh, UK. ¹³Department of Cognitive, Linguistic and Psychological Sciences, Brown University, Providence, RI, USA. Present address: ¹⁴Maurice Wohl Clinical Neuroscience Institute, Institute of Psychiatry, Psychology and Neuroscience, King's College London, London, UK. ¹⁵School of Biosciences, Dementia Research Institute, Cardiff University, Cardiff, UK. ¹⁶Centre for Neuroscience and Trauma, Blizzard Institute, Barts and the London School of Medicine and Dentistry, Queen Mary University of London, London, UK. ¹⁷These authors contributed equally: Matthew A. White and Eosu Kim. *e-mail: jemeen.sreedharan@kcl.ac.uk

including promoters and autoregulatory 3' UTR and maintaining the ubiquitous expression of TDP-43 during embryonic development and in adulthood. By avoiding deliberate manipulation of TDP-43 expression, this model helps elucidate both mediators and modifiers of cognitive dysfunction in ALS-FTD.

Results

TDP-43^{Q331K} causes behavioral phenotypes and disproportionately affects male mice. Over 50 *TARDBP* mutations at conserved sites have been identified in ALS-FTD¹¹. We chose to introduce the n.991 C>A (Q331K) mutation into murine *Tardbp* because TDP-43^{Q331K} is a particularly toxic species in vitro and in vivo^{4,9,12,13}. Mutagenesis was performed using CRISPR/Cas9 methodology, yielding four founders with the Q331K mutation (Fig. 1a). Mutagenesis events at predicted off-target regions and in the remainder of *Tardbp* were excluded by Sanger sequencing. Founder 52 was outcrossed to F₄ to remove other potential off-target mutagenesis events. Heterozygous (TDP-43^{Q331K/+}) F₄ animals were intercrossed to generate mutant and wild-type mice. Homozygotes (TDP-43^{Q331K/Q331K}) were viable (Fig. 1b and Supplementary Fig. 1a) and appeared superficially normal as juveniles. Since TDP-43 transgenic mice have not been shown to rescue TDP-43 knockout mice, TDP-43^{Q331K/Q331K} knock-in mice represent an opportunity to study mutant TDP-43 in vivo in the absence of wild-type TDP-43.

We initially screened for phenotypes in a small group of wild-type and TDP-43^{Q331K/Q331K} mice using automated continuous behavioral monitoring (ACBM)¹⁴. At ~4 months of age, TDP-43^{Q331K/Q331K} male and female mice demonstrated reduced walking and hanging

and increased rearing and eating by hand, but no alterations in circadian rhythmicity (Fig. 1c). The most consistent phenotype was reduced walking in males (Fig. 1d and Supplementary Fig. 1b). Further breeding revealed an under-representation of male mutants, yet females were present at Mendelian ratios, further suggesting that males are more susceptible to deleterious effects of TDP-43^{Q331K} (Fig. 1e). This is notable because sporadic ALS is more common in men, and TDP-43 mutations demonstrate greater penetrance in men than women¹⁵. We therefore focused on males in subsequent studies, breeding two cohorts of mice: cohort 1 for motor, pathological and transcriptomic studies, cohort 2 for cognitive studies.

TDP-43^{Q331K} mice display no significant motor impairment, but demonstrate weight gain due to hyperphagia and transcriptomic changes in spinal motor neurons.

To identify ALS-like motor deficits, we measured Rotarod performance in cohort 1 mice. From ~6 months of age, TDP-43^{Q331K/+} and TDP-43^{Q331K/Q331K} mice demonstrated reduced Rotarod latencies (Fig. 2a). Notably, mutants demonstrated hyperphagia, a feature of FTD¹⁶, and gained more weight than wild-type mice (Fig. 2b,c). Increased weight could contribute to impaired Rotarod performance, so we tested cohort 2 mice, which were weight-matched by dietary control (Supplementary Fig. 2a). Weight-matched mutants performed similarly to wild-type mice up to 16 months of age (Fig. 2d), suggesting that mutant mice do not have significant impairment of motor coordination.

To determine whether mutant mice demonstrate lower motor neuron degeneration, we examined spinal cords from 5-month-old mice to identify early pathological changes. Motor neurons

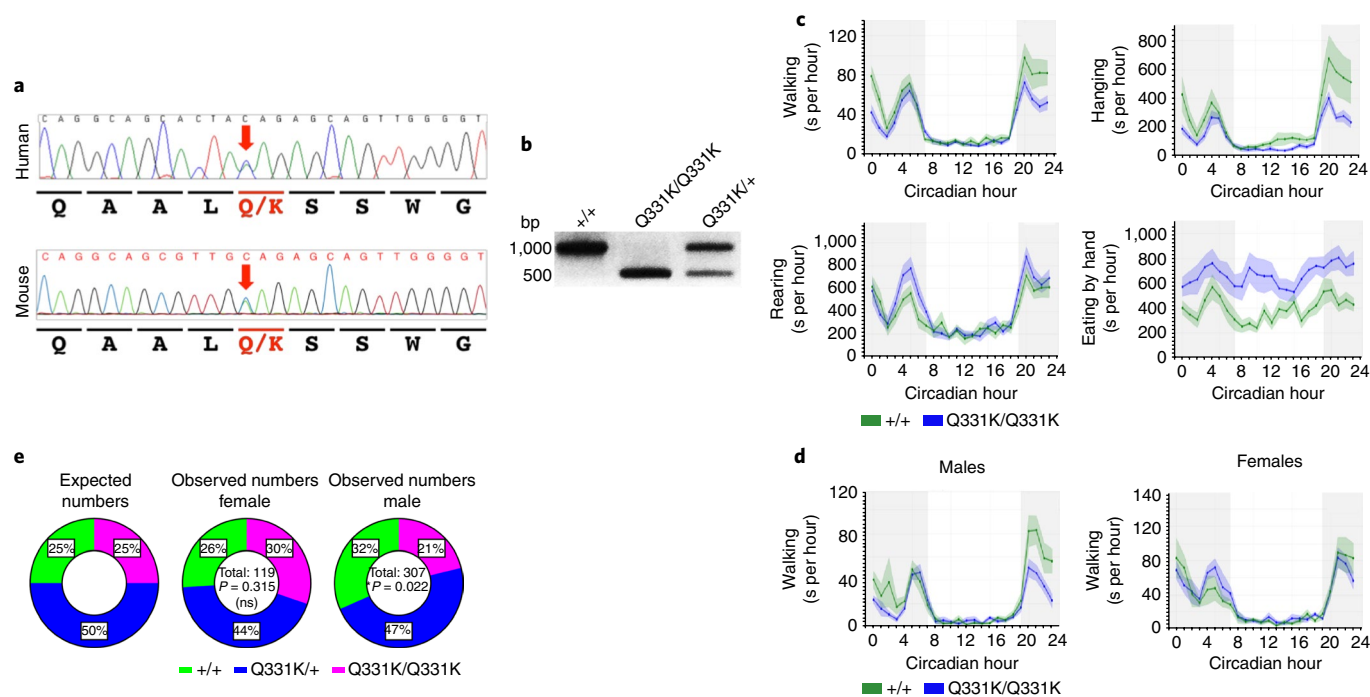


Fig. 1 | CRISPR mutagenesis, ACBM characterization and breeding ratios of TDP-43^{Q331K} mice. **a**, Chromatograms from the patient originally identified with the Q331K mutation and CRISPR/Cas9 knock-in founder mouse 52. Bases are given above the chromatograms and amino acids coded are given below. The mutation is highlighted with the red arrow. **b**, SaplI restriction enzyme digestion of 1,000-bp PCR products across the mutation site from representative genotyping of wild-type, TDP-43^{Q331K/Q331K} and TDP-43^{Q331K/+} mice. **c**, ACBM of 4-month-old mice (n=10 mice per genotype; 5 males and 5 females). Significantly altered behaviors are displayed: walking: interaction $P < 0.0001$; hanging: interaction $P = 0.002$; rearing: interaction $P = 0.038$; eating by hand: genotype $P = 0.008$; repeated measures two-way ANOVA. **d**, Walking behavior as assessed by ACBM in 7.5-month-old male and female mice (n=5 mice per genotype). Walking male: interaction $P < 0.0001$; walking female: interaction $P = 0.334$; repeated measures two-way ANOVA. **e**, Ratios of mice genotyped at 10 d (all of which were successfully weaned), by gender. Female: $\chi^2 = 2.311$, d.f. = 2, $P = 0.315$; male: $\chi^2 = 7.612$, d.f. = 2, $P = 0.022$; chi-squared test. Error bars represent mean \pm s.e.m.

demonstrated normal morphology and numbers, with no TDP-43 aggregation or mislocalization in TDP-43^{Q331K/Q331K} mice (Fig. 2e,f and Supplementary Fig. 2b). Quantification of neuromuscular junctions (NMJs) and succinate dehydrogenase staining in gastrocnemius muscles were normal in TDP-43^{Q331K/Q331K} mice, suggesting no significant denervation (Supplementary Fig. 2c,d,f). Examination of 18- to 23-month-old mice similarly found no evidence of denervation (Supplementary Fig. 2e) and no electrophysiological evidence of motor unit loss (Fig. 2g and Supplementary Fig. 2g–o).

Collectively, these data indicated a remarkable resilience of neuromuscular units to TDP-43^{Q331K}. We hypothesized that gene

expression changes occurring in motor neurons of mutant mice could elucidate how these cells respond to cellular stress caused by TDP-43^{Q331K}. We thus isolated RNA from laser-captured lumbar motor neurons from 5-month-old mice and performed RNA sequencing (RNA-seq; Supplementary Fig. 3a,b). This yielded 31 significant expression and splicing differences between wild-type and TDP-43^{Q331K/Q331K} mice (Fig. 2h,i, Supplementary Fig. 3c–e and Supplementary Table 1). A notable change was upregulation of agrin (*Agrn*). Agrin is secreted by neurons and functions through a muscle-specific kinase to cluster acetylcholine receptors at NMJs¹⁷. *Agrn* upregulation may therefore promote NMJ

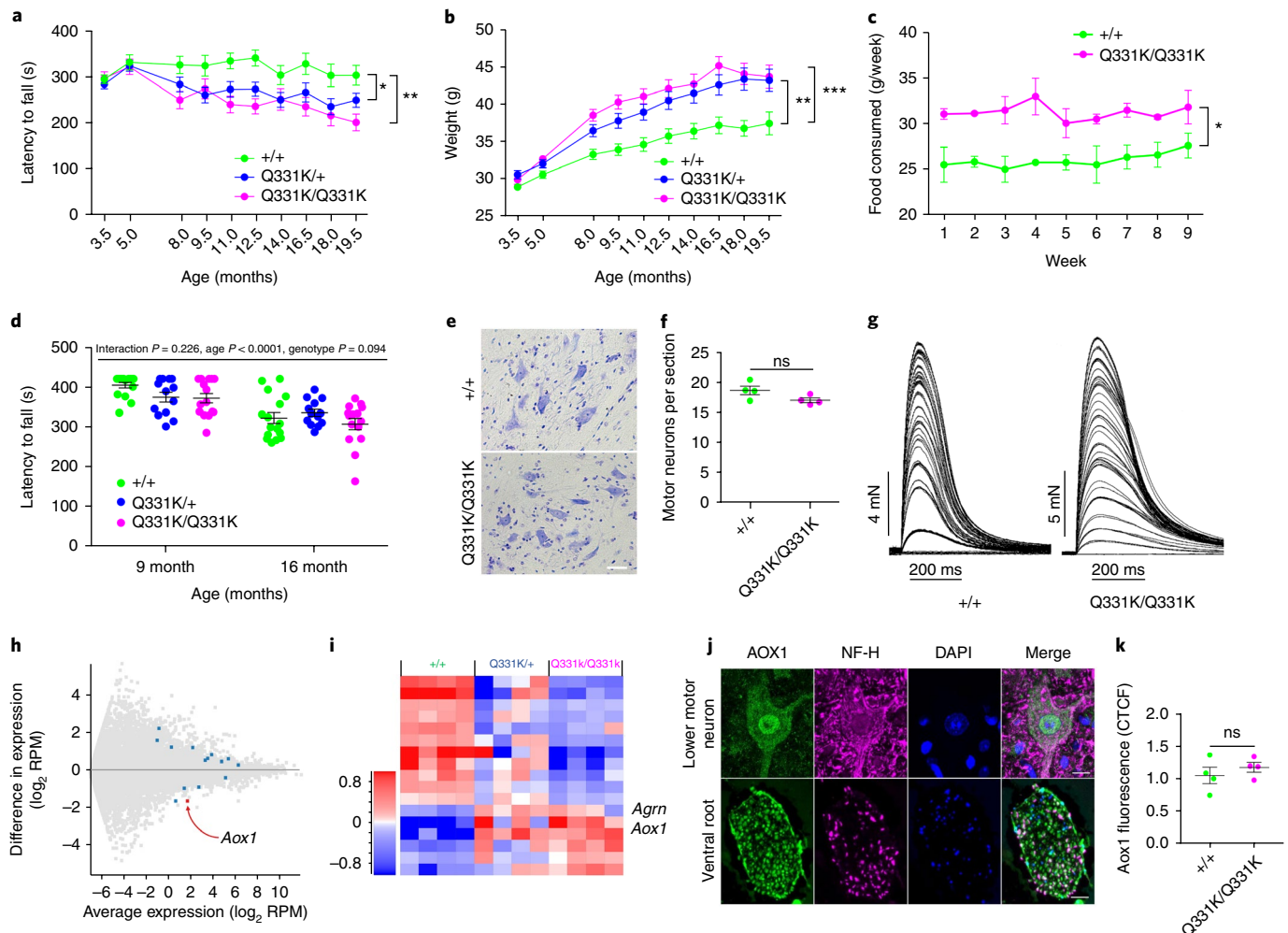


Fig. 2 | Motor impairment, hyperphagia and spinal motor neuronal transcriptomic changes in mutant mice. a,b, Rotarod (**a**) and weights (**b**) of cohort 1 mice ($n = 14$ wild-type, 13 TDP-43^{Q331K/+} and 13 TDP-43^{Q331K/Q331K} mice). **a**, Pairwise comparisons: wild-type vs. TDP-43^{Q331K/+}, $*P = 0.014$; wild-type vs. TDP-43^{Q331K/Q331K}, $**P = 0.0024$. **b**, Pairwise comparisons: wild-type vs. TDP-43^{Q331K/+}, $**P = 0.002$; wild-type vs. TDP-43^{Q331K/Q331K}, $***P = 0.0002$. **c**, Weekly food consumption over 9 weeks ($n = 2$ cages per genotype). Comparison: genotype: $*P = 0.047$. **d**, Rotarod of weight-matched cohort 2 mice ($n = 16$ wild-type, 13 TDP-43^{Q331K/+} and 15 TDP-43^{Q331K/Q331K} mice). For **a–d**, repeated measures two-way ANOVA followed by Holm–Sidak post hoc test for pairwise comparisons. **e**, Nissl-stained lumbar motor neurons of 5-month-old mice. Representative images shown. Scale bar, 40 μm . **f**, Quantification of lumbar motor neurons ($n = 4$ mice per genotype). Comparison: $P = 0.089$ (ns, not significant); unpaired *t*-test. **g**, Examples of isometric twitch force recordings during graded nerve stimulation of flexor digitorum brevis muscles from representative wild-type and TDP-43^{Q331K/Q331K} mice. Each increment corresponds to recruitment of motor units of successively higher electrical threshold ($n = 5$ mice per genotype). **h,i**, M (log ratio)–A (mean average) plot (**h**) and hierarchical clustering (**i**) of significantly differentially expressed genes (DEGs) in laser-captured motor neurons. RPM, reads per million reads of input. In **h**, blue dots indicate significant changes and red dots indicate intensity hits. In **i**, genes *Aox1* and *Agrn* are labeled. Comparison: DESeq2 (differential gene expression analysis based on negative binomial distribution) wild-type vs. TDP-43^{Q331K/Q331K}. **j**, Immunohistochemistry for AOX1, NF-H, neurofilament heavy chain. Representative images from a 5-month-old wild-type mouse shown. Scale bars, 10 μm motor neuron, 100 μm ventral root. **k**, AOX1 immunofluorescence in lumbar motor neurons. Comparison: $P = 0.433$ (ns); unpaired *t*-test. For **h–k**, $n = 4$ mice per genotype. All error bars denote mean \pm s.e.m.

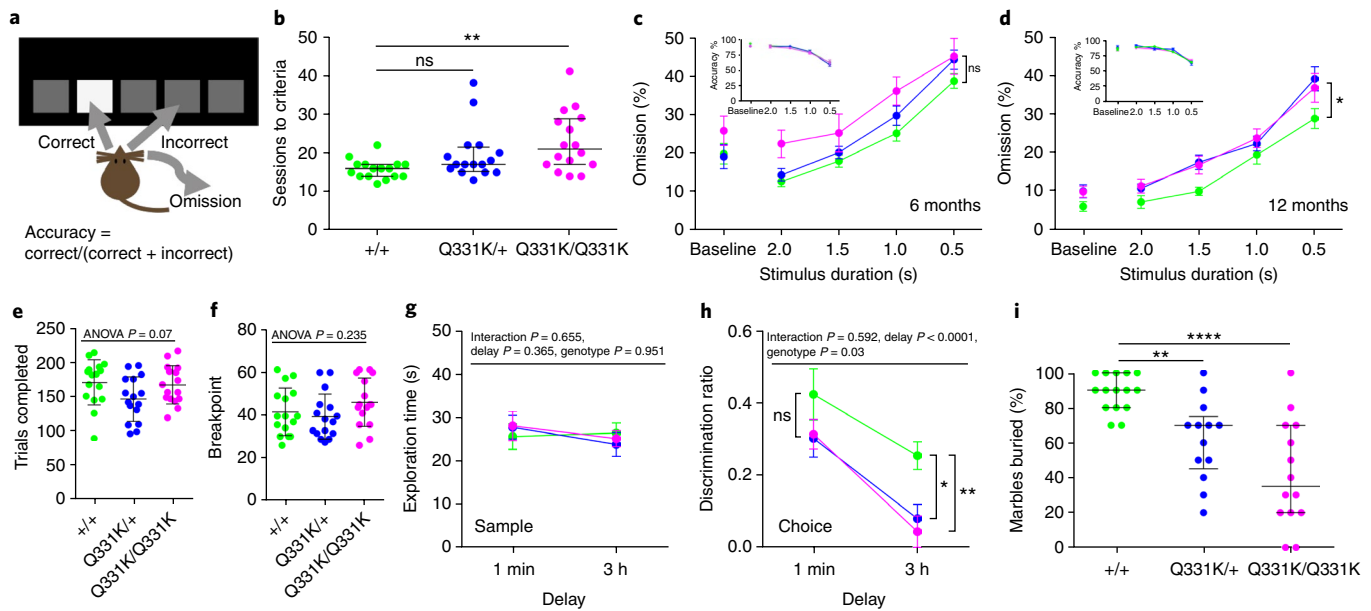


Fig. 3 | Cognitive testing indicates executive dysfunction, memory impairment and phenotypic heterogeneity in mutant mice. **a**, Schematic for the 5-CSRTT. **b**, Sessions required to reach performance criteria for 5-CSRTT ($n = 16$ per genotype). Pairwise comparisons: wild-type vs. TDP-43^{Q331K/+}; $P = 0.083$ (ns, not significant); wild-type vs. TDP-43^{Q331K/Q331K}; $**P = 0.004$. **c**, 5-CSRTT at 6 months of age ($n = 15$ wild-type, 16 TDP-43^{Q331K/+}, 15 TDP-43^{Q331K/Q331K} mice). Baseline session genotype effects: accuracy, $P = 0.109$; omission, $P = 0.283$. Stimulus duration (SD) probe test genotype effects: accuracy, $P = 0.833$; omission, $P = 0.077$ (ns); SD effect: accuracy and omission, $P < 0.001$; mixed-effects model. **d**, 5-CSRTT at 12 months of age ($n = 15$ wild-type, 16 TDP-43^{Q331K/+}, 16 TDP-43^{Q331K/Q331K} mice). Baseline session genotype effects: accuracy, $P = 0.487$; omission, $P = 0.120$. SD probe test genotype effects: accuracy, $P = 0.880$; omission, $*P = 0.044$; SD effect: accuracy, $P < 0.0001$; omission, $P < 0.0001$; genotype by SD interaction: accuracy, $P = 0.081$; omission, $P = 0.271$; mixed-effects model. **e**, Mean trials completed on an unrestricted fixed-ratio schedule (response increment per trial = 4; $n = 16$ per genotype). **f**, Mean breakpoint on a progressive-ratio schedule (response increment per trial = 4; $n = 16$ per genotype). **g, h**, Novel object recognition sample (**g**) and choice (**h**) phases ($n = 8$ wild-type, 9 TDP-43^{Q331K/+}, 8 TDP-43^{Q331K/Q331K} mice). For **h**, 1-min delay pairwise comparisons: wild-type vs. TDP-43^{Q331K/+}, $P = 0.158$ (ns); wild-type vs. TDP-43^{Q331K/Q331K}, $P = 0.158$ (ns); 3-h delay pairwise comparisons: wild-type vs. TDP-43^{Q331K/+}, $*P = 0.014$; wild-type vs. TDP-43^{Q331K/Q331K}, $**P = 0.009$. For **b, e, f** one-way ANOVA and for **g, h** two-way ANOVA, all followed by Holm-Sidak post hoc tests for pairwise comparisons. **i**, Marbles buried by cohort 1 at 18 months of age ($n = 15$ wild-type, 13 TDP-43^{Q331K/+}, 14 TDP-43^{Q331K/Q331K} mice). Pairwise comparisons: wild-type vs. TDP-43^{Q331K/+}, $**P = 0.009$; wild-type vs. TDP-43^{Q331K/Q331K}, $****P < 0.0001$; Kruskal-Wallis followed by Dunn's test for pairwise comparisons. Error bars denote s.e.m. for **c–h** and median and interquartile range for **b** and **i**.

function in TDP-43^{Q331K/Q331K} mice. The largest gene expression change was a threefold increase in expression of aldehyde oxidase 1 (*Aox1*). Little is known about the neurobiological functions of AOX1, although its transcript has been observed in the anterior horn of the spinal cord¹⁸. AOX1 catalyzes the conversion of retinaldehyde to retinoic acid^{19–21}, which functions in neuronal maintenance in the adult nervous system and following axon injury. Thus, *Aox1* upregulation may benefit motor neurons in TDP-43^{Q331K/Q331K} mice. Immunostaining revealed expression of AOX1 in spinal motor neurons (Fig. 2j), but no difference in expression between TDP-43^{Q331K/Q331K} and wild-type mice (Fig. 2k and Supplementary Fig. 3f). This could be because upregulated AOX1 is transported into peripheral motor axons, as we found abundant expression of AOX1 in motor axons (Fig. 2j).

TDP-43^{Q331K} mice display executive dysfunction, memory impairment and phenotypic heterogeneity. In parallel with motor studies, to determine whether TDP-43^{Q331K} causes FTD-like cognitive dysfunction we performed neuropsychological assessments on cohort 2 mice using touchscreen operant technology. To test whether mice exhibited FTD-related deficits, we used the five-choice serial reaction time task (5-CSRTT; Fig. 3a), which measures frontal or executive function, including attention, perseveration, impulsivity and psychomotor speed²². At 4 months of age the number of training sessions required to reach performance criteria for probe testing was higher in TDP-43^{Q331K/Q331K} mice than wild-type mice (Fig. 3b),

indicating learning deficits in mutants. Following training, animals underwent probe testing at 6 and 12 months of age. Accuracy (Fig. 3c,d, insets) and omission percentage were comparable between genotypes at 6 months of age (Fig. 3c). However, at 12 months of age, while accuracy remained normal, omission percentage was greater in TDP-43^{Q331K/+} and TDP-43^{Q331K/Q331K} mice (Fig. 3d), suggesting attentional deficits and cognitive decline in mutants. Reward collection and response latencies, as well as premature and perseverative response rates, were similar between genotypes (Supplementary Fig. 4a–h), arguing against visual, motivational or significant motor deficits as causes for increased omissions. We also measured motivation using fixed-ratio and progressive-ratio schedules. No significant differences were found between genotypes, further suggesting that increased omissions in mutants were not due to motivational deficits (Fig. 3e,f). Collectively, these data indicate an inattention phenotype in TDP-43^{Q331K/+} and TDP-43^{Q331K/Q331K} mice, which is consistent with frontal or executive dysfunction.

Next, to explore temporal-lobe-dependent function, we conducted the spontaneous object recognition task, a test of declarative memory. Initial exploratory times did not differ between genotypes (Fig. 3g), but in the choice phase a deficit emerged in TDP-43^{Q331K/+} and TDP-43^{Q331K/Q331K} mice (Fig. 3h), indicating memory impairment. The combination of executive dysfunction and memory impairment, together with hyperphagia in free-fed cohort 1 mice, led us to conclude that TDP-43^{Q331K/+} and TDP-43^{Q331K/Q331K} mice recapitulate FTD at the behavioral level.

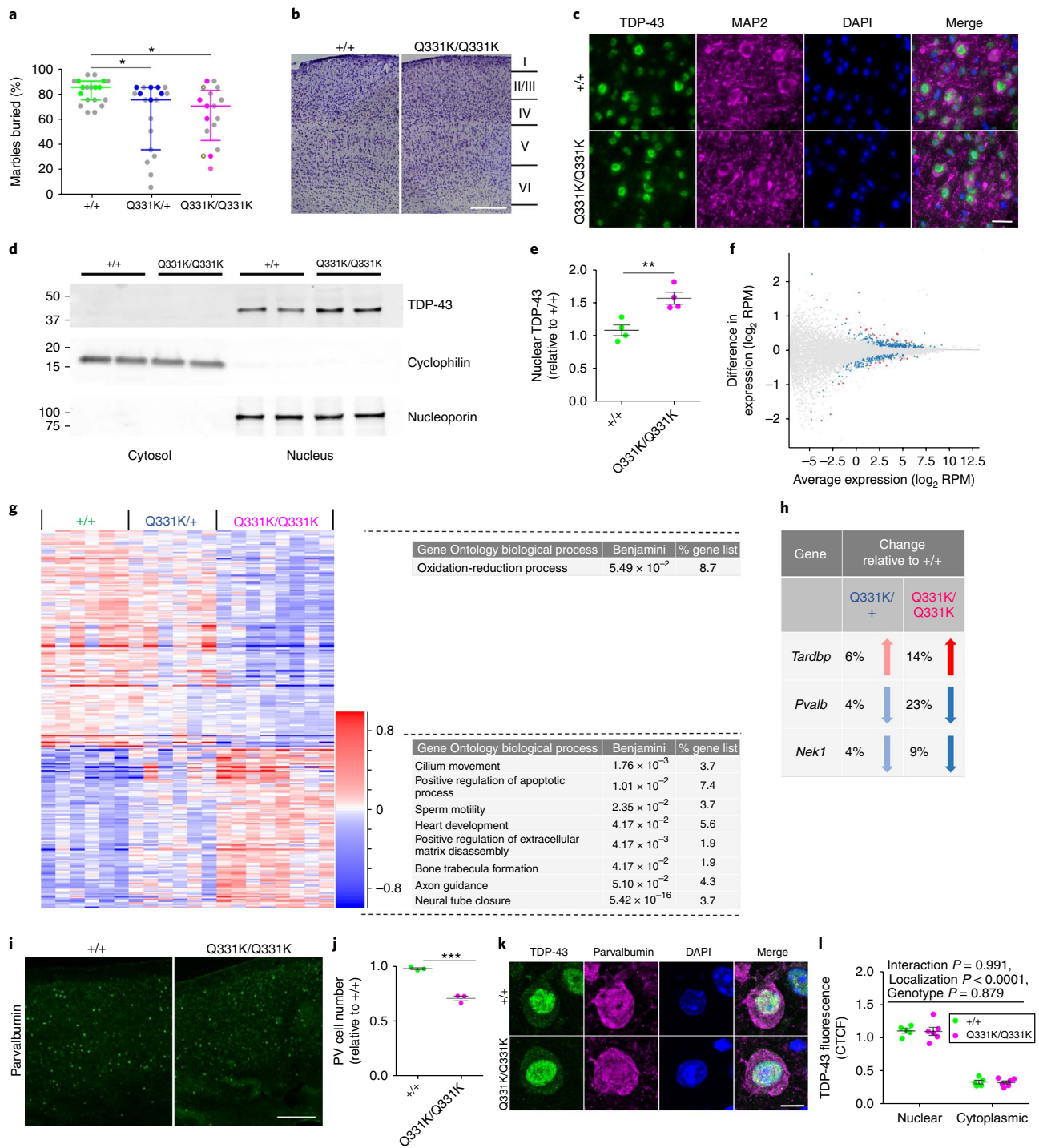


Fig. 4 | Perturbed TDP-43 autoregulation and loss of parvalbumin interneurons in mutant mice. a, Marbles buried by 5-month-old mice. Colored dots indicate animals used for RNA-seq analysis. Yellow dots indicate TDP-43^{Q331K/Q331K} littermates ($n=19$ wild-type, 19 TDP-43^{Q331K/+}, 17 TDP-43^{Q331K/Q331K} mice). Pairwise comparisons: wild-type vs. TDP-43^{Q331K/+}, $*P=0.028$; wild-type vs. TDP-43^{Q331K/Q331K}, $*P=0.013$; Kruskal-Wallis followed by Dunn's test for pairwise comparisons. Error bars represent median and interquartile range. **b**, Representative Nissl staining of frontal cortex (layers indicated) ($n=5$ wild-type, 6 TDP-43^{Q331K/Q331K} mice). Scale bar, 500 μm . **c**, Immunohistochemistry for TDP-43 in pyramidal neurons of motor cortex layer V. Representative images shown ($n=4$ mice per genotype). MAP2, microtubule-associated protein 2. Scale bar, 20 μm . **d**, Immunoblot of fractionated frontal cortical tissue from 5-month-old mice (two biological replicates shown, uncropped in Supplementary Fig. 5). **e**, Immunoblot band intensity quantification ($n=4$ mice per genotype). Comparison: $**P=0.007$; unpaired t -test. Error bars denote s.e.m. **f, g**, MA plot (**f**) and hierarchical clustering (**g**) of DEGs ($n=6$ wild-type, 6 TDP-43^{Q331K/+}, 8 TDP-43^{Q331K/Q331K} mice) in frontal cortex. For **f**, blue dots indicate significant changes and red dots indicate intensity hits. Comparison: DESeq2 wild-type vs. TDP-43^{Q331K/Q331K}. For **g**, Gene Ontology biological process and KEGG pathway enriched terms are displayed. **h**, Expression changes for parvalbumin and ALS-FTD linked genes identified by RNA-seq. **i**, Immunohistochemistry for parvalbumin in cortices of 5-month-old mice. Representative images shown. Scale bar, 250 μm . **j**, Quantification of parvalbumin-positive (PV) neurons ($n=3$ mice per genotype). Comparison: $***P=0.0003$; unpaired t -test. Error bars denote s.e.m. **k**, Immunohistochemistry for TDP-43 in parvalbumin-positive cells. Representative images shown. Scale bar, 5 μm . **l**, TDP-43 expression in parvalbumin-positive cells ($n=5$ mice per genotype). Comparison by two-way ANOVA. Error bars denote s.e.m.

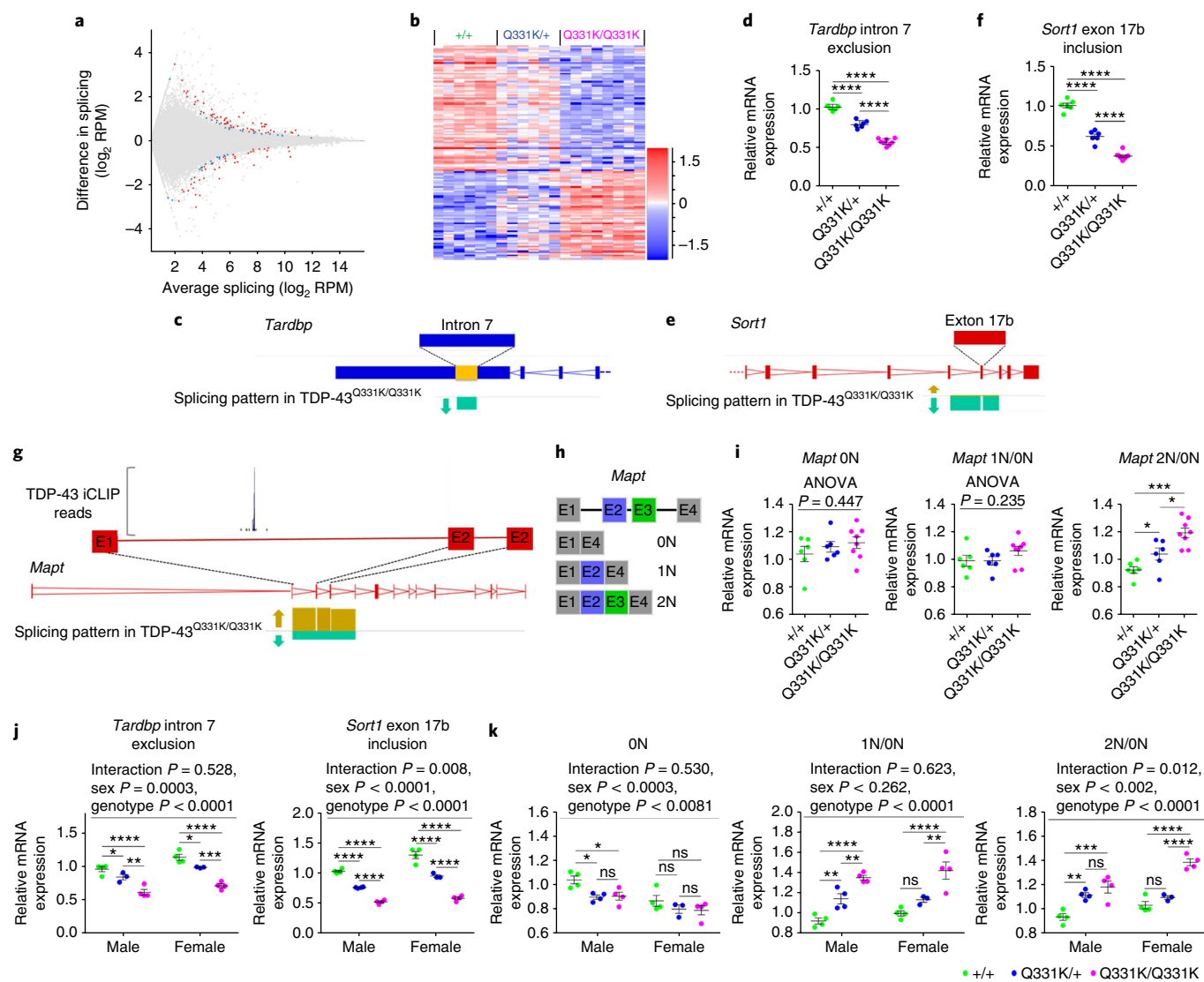


Fig. 5 | Splicing analysis indicates TDP-43 misregulation, a gain of TDP-43 function and altered *Mapt* exon 2/3 splicing. **a, b**, MA plot (**a**) and hierarchical clustering (**b**) of frontal cortical alternative splice events ($n = 6$ wild-type, 6 TDP-43^{Q331K/+}, 8 TDP-43^{Q331K/Q331K} mice). Comparison: DESeq2 wild-type vs. TDP-43^{Q331K/Q331K}. **c**, Schematic of altered splicing in the 3' UTR of *Tardbp*. Arrow indicates reduced exclusion of intron 7 of the *Tardbp* transcript in TDP-43^{Q331K/Q331K} relative to wild-type mice. **d**, Quantitative PCR (qPCR) of splicing changes in *Tardbp* intron 7 ($n = 6$ wild-type, 6 TDP-43^{Q331K/+}, 8 TDP-43^{Q331K/Q331K} mice). **e**, Schematic of exon 17b inclusion or exclusion in *Sort1*. Arrows indicate reduced inclusion of exon 17b in TDP-43^{Q331K/Q331K} relative to wild-type mice. **f**, qPCR of splicing changes in *Sort1* exon 17b ($n = 6$ wild-type, 6 TDP-43^{Q331K/+}, 8 TDP-43^{Q331K/Q331K} mice). **g**, Schematic of altered splicing of exons 2 and 3 of *Mapt*. Arrows indicate increased inclusion of exons 2 and 3 in the *Mapt* transcripts from TDP-43^{Q331K/Q331K} relative to wild-type mice. The expanded view of exon 1 to exon 2 includes a site of TDP-43 binding as detected by iCLIP (iCount pipeline; TDP-43_CLIP_E18-brain). **h**, Schematic of N-terminal *Mapt* splice variants (ON, 1N and 2N). **i**, qPCR of splicing changes in *Mapt* exons 2 and 3 ($n = 6$ wild-type, 6 TDP-43^{Q331K/+}, 8 TDP-43^{Q331K/Q331K} mice). 2N/ON pairwise comparisons: wild-type vs. TDP-43^{Q331K/+}, $*P = 0.047$; wild-type vs. TDP-43^{Q331K/Q331K}, $***P = 0.0001$; TDP-43^{Q331K/+} vs. TDP-43^{Q331K/Q331K}, $*P = 0.013$. **j, k**, qPCR of hippocampal splicing changes ($n = 4$ wild-type, 3 TDP-43^{Q331K/+}, 4 TDP-43^{Q331K/Q331K} mice per gender). Pairwise comparisons: *Tardbp* intron 7 exclusion, male wild-type vs. TDP-43^{Q331K/+}, $*P = 0.043$; male TDP-43^{Q331K/+} vs. TDP-43^{Q331K/Q331K}, $***P = 0.002$; female wild-type vs. TDP-43^{Q331K/+}, $*P = 0.013$; female TDP-43^{Q331K/+} vs. TDP-43^{Q331K/Q331K}, $***P = 0.0002$; *Sort1*: ON, male: wild-type vs. TDP-43^{Q331K/+}, $*P = 0.023$; wild-type vs. TDP-43^{Q331K/Q331K}, $*P = 0.023$; TDP-43^{Q331K/+} vs. TDP-43^{Q331K/Q331K}, $P = 0.877$ (ns, not significant); female: wild-type vs. TDP-43^{Q331K/+}, $P = 0.365$ (ns); wild-type vs. TDP-43^{Q331K/Q331K}, $P = 0.324$ (ns); TDP-43^{Q331K/+} vs. TDP-43^{Q331K/Q331K}, $P = 0.858$ (ns); 1N/ON, male: wild-type vs. TDP-43^{Q331K/+}, $**P = 0.008$; TDP-43^{Q331K/+} vs. TDP-43^{Q331K/Q331K}, $**P = 0.008$; female: wild-type vs. TDP-43^{Q331K/+}, $P = 0.077$ (ns); TDP-43^{Q331K/+} vs. TDP-43^{Q331K/Q331K}, $**P = 0.002$; 2N/ON, male: wild-type vs. TDP-43^{Q331K/+}, $***P = 0.002$; wild-type vs. TDP-43^{Q331K/Q331K}, $***P = 0.0001$; TDP-43^{Q331K/+} vs. TDP-43^{Q331K/Q331K}, $P = 0.151$ (ns); female: wild-type vs. TDP-43^{Q331K/+}, $P = 0.202$ (ns). For **d, f, i, k**, $****P < 0.0001$. For **d, f, i**, one-way and for **j, k** two-way ANOVA, all followed by Holm-Sidak post hoc tests for pairwise comparisons. Error bars denote s.e.m.

During touchscreen analyses we noted that some cohort 2 mutant mice demonstrated consistently worse performance than other mutants (Fig. 3b and Supplementary Fig. 4i). This phenotypic heterogeneity was intriguing given that the mutant mice were genetically homogeneous. Furthermore, ALS-FTD is a remarkably

heterogeneous disease in which patients display varying phenotypic severity and different rates of disease progression. Indeed, *TARDBP* mutation carriers demonstrate variable penetrance even with homozygous mutations¹⁵. We therefore looked for further evidence of phenotypic heterogeneity by examining cohort 1 mice

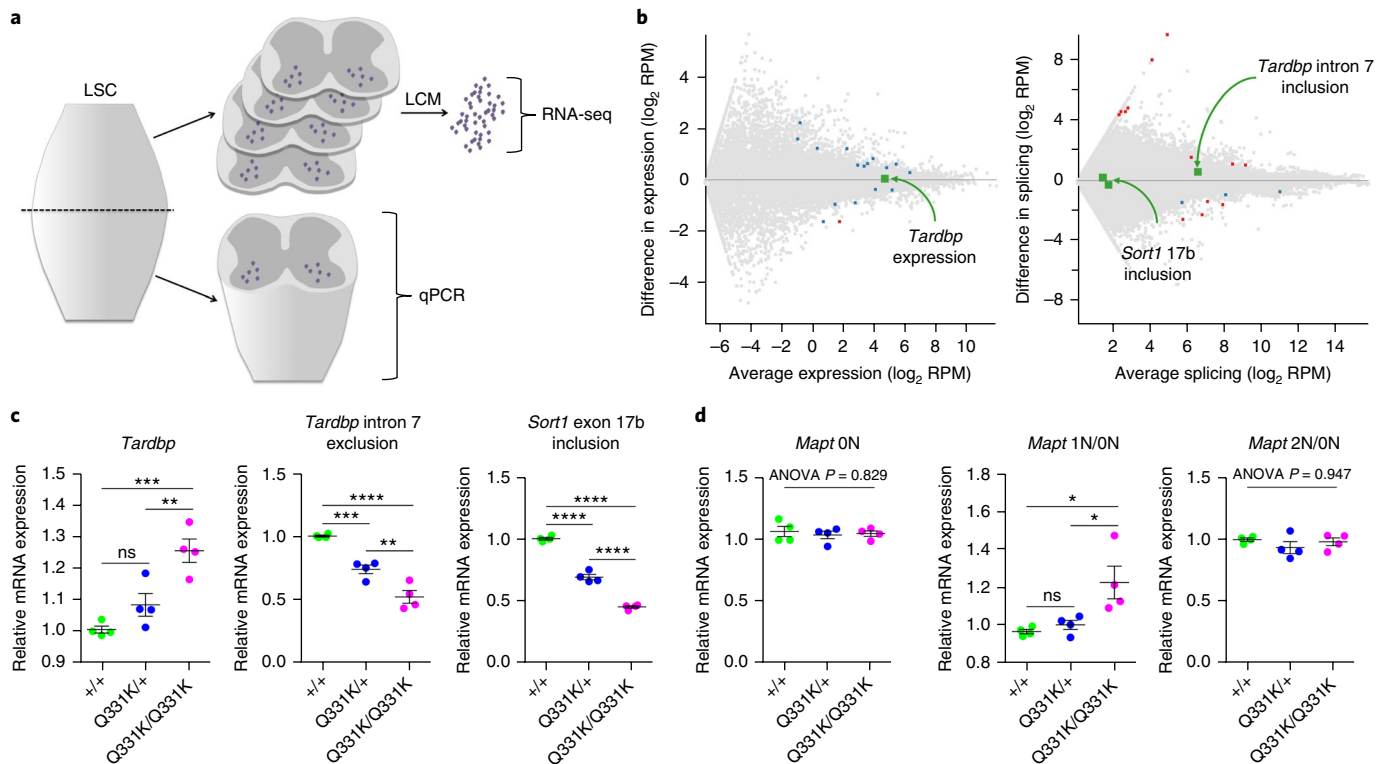


Fig. 6 | TDP-43 misregulation occurs in spinal cords of mutant mice, but not in motor neurons. **a**, Schematic detailing lumbar spinal cord (LSC) processing for transcriptomic analysis (LCM, laser capture microdissection). **b**, MA plots of lumbar motor neuron differentially expressed and spliced genes ($n = 4$ mice per genotype). Comparison: DESeq2 wild-type vs. TDP-43^{Q331K/Q331K}. Blue dots indicate significant changes and red dots indicate intensity hits. Green dots highlight *Tardbp* expression, *Tardbp* intron 7 exclusion and *Sort1* exon 17b inclusion, which are not significant changes. **c,d**, Quantitative PCR of homogenized lumbar spinal cord ($n = 4$ wild-type, 4 TDP-43^{Q331K/+}, 4 TDP-43^{Q331K/Q331K} mice). Comparisons as follows: **c**, *Tardbp* expression: wild-type vs. TDP-43^{Q331K/+}, $P = 0.103$ (ns, not significant); wild-type vs. TDP-43^{Q331K/Q331K}, $***P = 0.0008$; TDP-43^{Q331K/+} vs. TDP-43^{Q331K/Q331K}, $**P = 0.007$. *Tardbp* intron 7 exclusion: wild-type vs. TDP-43^{Q331K/+}, $***P = 0.001$; wild-type vs. TDP-43^{Q331K/Q331K}, $****P < 0.0001$; TDP-43^{Q331K/+} vs. TDP-43^{Q331K/Q331K}, $***P = 0.002$. *Sort1* exon 17b inclusion: $****P < 0.0001$. **d**, *Mapt* splice variant expression: 0N *Mapt*; 1N *Mapt*: wild-type vs. TDP-43^{Q331K/+}, $P = 0.640$ (ns); wild-type vs. TDP-43^{Q331K/Q331K}, $*P = 0.02$; TDP-43^{Q331K/+} vs. TDP-43^{Q331K/Q331K}, $*P = 0.03$; 2N *Mapt*. **c,d**, Comparisons by one-way ANOVA followed by Holm-Sidak post hoc tests. Error bars denote s.e.m.

using the marble-burying assay, a measure of innate digging behavior²³. From 5 to 18 months of age, wild-type mice buried ~80% of marbles. Mutants demonstrated a range of digging behaviors, with some animals behaving similarly to wild-type mice but others demonstrating attenuated digging behavior (Fig. 3i and Supplementary Fig. 4j). These observations confirm the presence of phenotypic heterogeneity in genetically homogeneous groups of mutant mice and suggest that some mutants were relatively resistant to behavioral deficits caused by TDP-43^{Q331K}.

TDP-43^{Q331K} mice demonstrate perturbed TDP-43 autoregulation and reduced parvalbumin-positive neurons. To obtain mechanistic insight into the cognitive dysfunction in TDP-43^{Q331K} mice, we conducted pathological and transcriptomic studies at 5 months of age. We first performed the marble-burying assay to identify animals with a range of different behaviors (Fig. 4a). Analysis of frontal cortices from wild-type and TDP-43^{Q331K/Q331K} mice demonstrated no significant reduction in cortical thickness or cellular density in mutants (Fig. 4b and Supplementary Fig. 5a–c), and no nuclear clearing or cytoplasmic aggregation of TDP-43 (Fig. 4c). However, subcellular fractionation and immunoblotting demonstrated a ~45% increase in nuclear TDP-43 in TDP-43^{Q331K/Q331K} compared to wild-type mice (Fig. 4d,e and Supplementary Fig. 5d).

TDP-43 has critical roles in RNA processing, which may be disturbed in disease. We therefore performed transcriptomic

analyses using RNA-seq of frontal cortices from six wild-type, six TDP-43^{Q331K/+} and eight TDP-43^{Q331K/Q331K} mice (Supplementary Fig. 6a). We identified 171 genes that were upregulated and 233 that were downregulated in TDP-43^{Q331K/Q331K} mice relative to wild-type (Fig. 4f,g). TDP-43^{Q331K/+} mice demonstrated changes that trended in the same direction as TDP-43^{Q331K/Q331K} mice, suggesting a dose-dependent effect of the mutation. In particular, we noted a 14% increase in expression of *Tardbp* in TDP-43^{Q331K/Q331K} mice (Fig. 4h). As nuclear TDP-43 protein expression was also elevated in mutants, we conclude that the Q331K mutation disturbs TDP-43 autoregulation.

One notable gene that was downregulated in mutant mice was *Nek1*. This change is consistent with human data indicating that loss-of-function mutations in *NEK1* cause ALS^{24,25}. Another downregulated gene was *Pvalb*, which encodes the calcium buffering protein parvalbumin. Reduced parvalbumin immunopositivity is observed in patients with ALS and is linked with selective cellular vulnerability in ALS²⁶. We therefore immunostained for parvalbumin and found a ~25% reduction in parvalbumin-positive cells in the frontal cortex of TDP-43^{Q331K/Q331K} mice (Fig. 4i,j). Co-staining for TDP-43 in this affected subset of cortical neurons did not demonstrate TDP-43 mislocalization (Fig. 4k,l). Notably, fast-spiking parvalbumin interneurons are GABAergic inhibitory cells that play a direct role in the control of attention²⁷. We therefore conclude that a paucity of parvalbumin interneurons may be responsible for the attentional impairment of TDP-43^{Q331K} mice.

Splicing analysis indicates a gain of function of TDP-43^{Q331K} and links aberrant TDP-43 homeostasis with altered splicing of *Mapt*. TDP-43 plays key roles in alternative splicing. We therefore

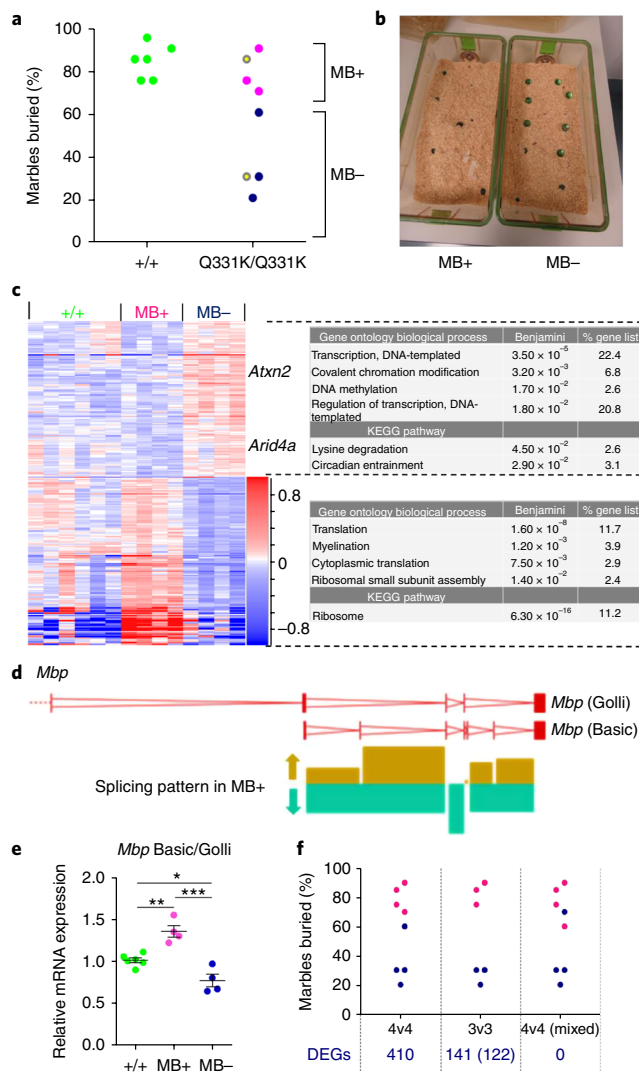


Fig. 7 | Phenotypic stratification of transcriptomic data from mutant mice allows the identification of putative disease modifiers. **a**, Marble-burying in 5-month-old mice before transcriptomic analysis. MB+ mice bury at or above the median number of marbles for the group, and MB- mice bury fewer. Yellow dots indicate TDP-43^{Q331K/Q331K} littermates. **b**, Marble burying activity of the TDP-43^{Q331K/Q331K} littermates indicated in **a**. **c**, Hierarchical clustering of DEGs in frontal cortices comparing MB+ and MB- TDP-43^{Q331K/Q331K} mice. Genes *Atxn2* and *Arid4a* are highlighted ($n=6$ wild-type, 4 MB+ TDP-43^{Q331K/Q331K} and 4 MB- TDP-43^{Q331K/Q331K} mice). Comparison: DESeq2 MB+ vs. MB-. Gene Ontology biological processes and KEGG pathway enriched terms are displayed. **d**, Graphical representation of altered splicing of *Mbp*. Arrows indicate the altered pattern of splicing in MB+ relative to MB- TDP-43^{Q331K/Q331K} mice. **e**, qPCR of the ratio of *Mbp* Basic to *Mbp* Golli ($n=6$ wild-type, 4 TDP-43^{Q331K/+}, 4 TDP-43^{Q331K/Q331K} mice). Pairwise comparisons: wild-type vs. MB+, $**P=0.005$; wild-type vs. MB-, $*P=0.024$; MB+ vs. MB-, $***P=0.0003$; one-way ANOVA followed by Holm-Sidak post hoc tests. Error bars denote s.e.m. **f**, Representative marble burying analyses: 4v4, original analysis; 3v3, comparing the three best MB+ and three worst MB- mice; 4v4 mixed, one MB- mouse swapped with one MB+ mouse. Number of DEGs identified by DESeq2 comparison of MB+ vs. MB- mice for each comparison is given below. For 3v3, hits common to those of the 4v4 stratification are shown in parentheses.

interrogated the cortical transcriptomic dataset further for splicing differences between mutant and wild-type mice and identified 138 splicing changes in 106 genes (Fig. 5a,b and Supplementary Fig. 6b). This included an ~80% increase in retention of *Tardbp* intron 7 in TDP-43^{Q331K/Q331K} mice (Fig. 5c,d), which will promote the production of stable mRNA species⁷. This confirms that TDP-43 autoregulation is perturbed in mutant mice. Another prominent change was a 2.4-fold increase in exclusion of *Sort1* exon 17b, a known splicing target of TDP-43 (Fig. 5e,f). This change is consistent with a gain of function of TDP-43²⁸.

We also noted altered splicing of exons 2 and 3 of *Mapt*, which encodes the microtubule associated protein tau and is mutated in FTD with parkinsonism²⁹. We detected increased inclusion of *Mapt* exons 2 and 3 in TDP-43^{Q331K/Q331K} mice (Fig. 5g-i). This is notable because inclusion of exons 2 and 3 of *Mapt* is associated with increased somatodendritic localization and aggregation of tau³⁰. We immunostained wild-type and mutant frontal cortices for total tau but found no difference in the localization or aggregation of tau (Supplementary Fig. 6c). Analysis of iCLIP databases (<http://icount.biobab.si/groups.html>) revealed that TDP-43 binds to an intronic sequence upstream of *Mapt* exon 2 (Fig. 5g). This confirmed that *Mapt* exons 2 and 3 are likely splicing targets of TDP-43. The identification of this splicing effect of TDP-43 on *Mapt* mechanistically links these two major dementia genes.

Next, to determine whether TDP-43 misregulation could be responsible for temporal-lobe-dependent functions, we analyzed hippocampal RNA extracts from male mice. We also examined hippocampi from female mice to determine whether TDP-43 misregulation was restricted to male mice. Splicing analyses for *Tardbp*, *Sort1* and *Mapt* were consistent with a gain of function of TDP-43 in mutant mice of both genders (Fig. 5j,k). This indicates that TDP-43 misregulation occurs beyond the frontal cortex, and in both male and female mice.

Finally, to confirm that our behavioral and transcriptomic observations were caused by mutant TDP-43 and not off-target CRISPR mutagenesis effects, we performed the marble-burying assay in a second line of TDP-43^{Q331K} knock-in mice, line 3, and found a similar impairment of digging behavior to line 52 mice (Supplementary Fig. 6d). We also analyzed RNA from line 3 mice and observed an increase in *Tardbp* expression and altered splicing of *Tardbp* and *Sort1*, which is consistent with perturbed autoregulation and a gain of function of TDP-43 (Supplementary Fig. 6e). Furthermore, line 3 TDP-43^{Q331K/Q331K} mice also demonstrated increased inclusion of exons 2 and 3 of *Mapt* and a paucity of parvalbumin-positive neurons relative to wild-type mice, replicating key splicing and pathological observations made in line 52 mice (Supplementary Fig. 6e,f).

TDP-43 misregulation in lumbar spinal cords of mutant mice further implicates interneurons in ALS-FTD pathogenesis. Our transcriptomic profiling of frontal cortices and hippocampi elucidated a gain of function of TDP-43 in the brains of mutant mice. By contrast, spinal motor neurons from mutants did not demonstrate TDP-43 misregulation, as *Tardbp*, *Sort1* and *Mapt* were not differentially expressed or spliced in these cells (Fig. 6b). However, TDP-43 misregulation could occur in other cells of the spinal cord, namely glia or interneurons. We therefore analyzed RNA from homogenates of lumbar spinal cord from the mice from which we had laser captured spinal motor neurons (Fig. 6a). Notably, spinal cord homogenates demonstrated increased expression of *Tardbp* and altered splicing of *Tardbp* and *Sort1* consistent with a gain of function of TDP-43 in mutant mice (Fig. 6c). Furthermore, spinal cords from mutant mice also demonstrated increased inclusion of *Mapt* exon 2 (Fig. 6d). Given that *Mapt* expression is predominantly neuronal rather than glial, this suggests that a gain of TDP-43 function occurs in interneurons of the spinal cord.

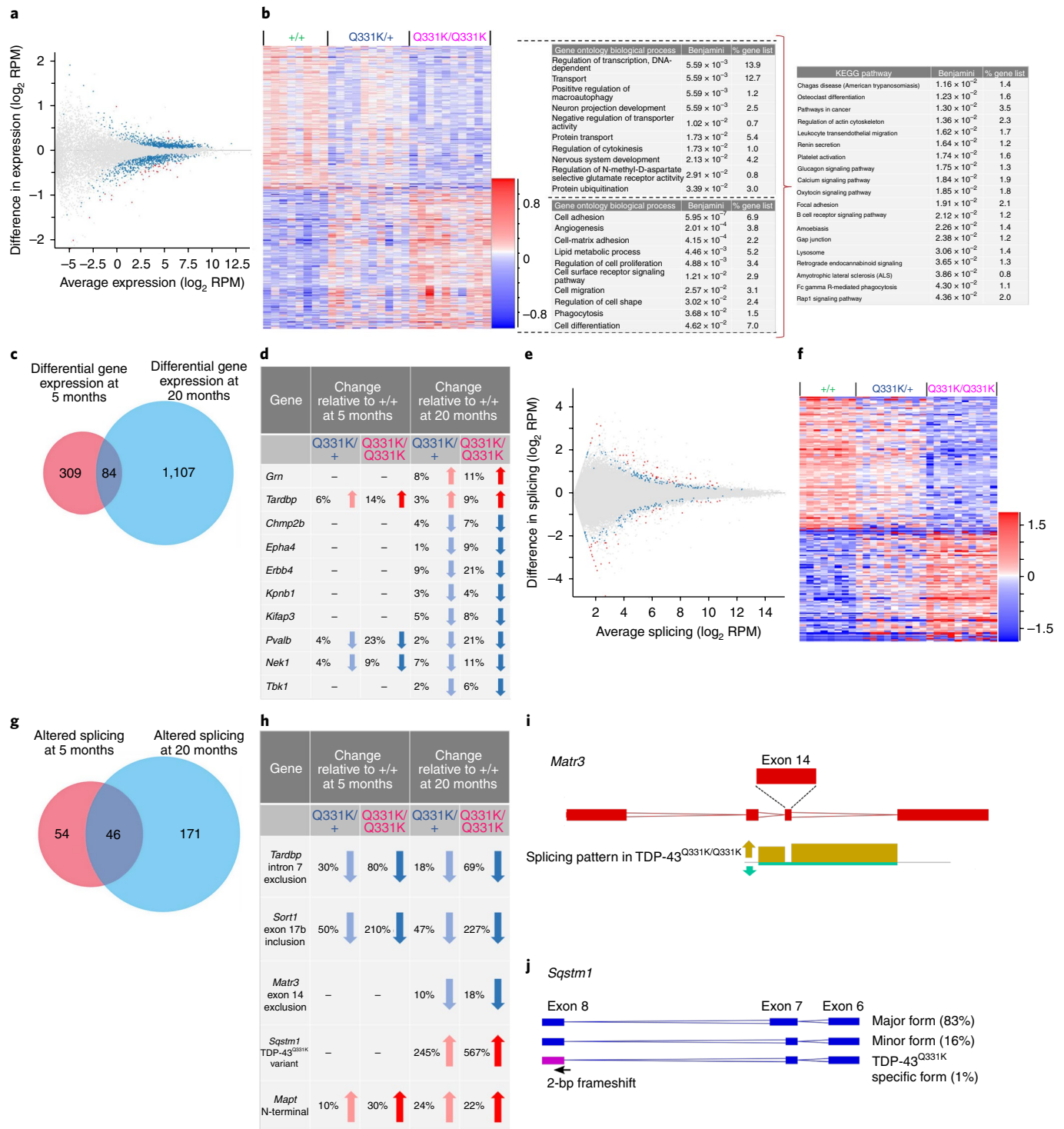


Fig. 8 | TDP-43^{Q331K} mice demonstrate age-related deterioration in cortical transcriptomes with altered expression of multiple ALS-linked genes. a,b, MA plot (**a**) and hierarchical clustering (**b**) of DEGs in frontal cortices at 20 months of age. For **a**, blue dots indicate significant changes and red dots indicate intensity hits. Comparison: DESeq2 wild-type vs. TDP-43^{Q331K/Q331K}. For **b**, Gene Ontology biological processes and KEGG pathway enriched terms are displayed. **c**, Venn diagram highlighting DEGs between wild-type vs. TDP-43^{Q331K/Q331K} mice that were common to analyses in 5- and 20-month-old mice. Known ALS-FTD linked genes in this common subset are highlighted in **d**. **e,f**, MA plot (**e**) and hierarchical clustering (**f**) of frontal cortical alternative splice events at 20 months of age. Blue dots indicate significant changes and red dots indicate intensity hits. Comparison: DESeq2 wild-type vs. TDP-43^{Q331K/Q331K}. For **a,b,e,f** $n = 8$ wild-type, 10 TDP-43^{Q331K/+}, 10 TDP-43^{Q331K/Q331K} mice. **g**, Venn diagram highlighting alternative splice events between wild-type vs. TDP-43^{Q331K/Q331K} mice that are common to analyses in 5- and 20-month-old mice. **h**, Known ALS-FTD linked genes in this common subset. **i**, Schematic of *Matr3* exon 14 inclusion and exclusion. Arrows indicate increased inclusion of exon 14 in TDP-43^{Q331K/Q331K} relative to wild-type mice. **j**, Schematic of *Sqstm1* transcript splice variants. Percentages given indicate the relative amount of each variant in TDP-43^{Q331K/Q331K} mice. The TDP-43^{Q331K}-specific variant is undetectable in wild-type mice.

Stratification of transcriptomic data from TDP-43^{Q331K/Q331K} mice by phenotype identifies expression and splicing changes.

As stated earlier, some mutant mice appeared relatively resistant to the cognitive effects of the Q331K mutation. We wished to exploit this phenotypic heterogeneity in TDP-43^{Q331K/Q331K} mice to identify potential modifiers of cognitive dysfunction. For this purpose, we divided the frontal cortical transcriptomic data from the eight TDP-43^{Q331K/Q331K} mice into two subsets according to their antemortem marble-burying behavior. We designated this the 'MB +/-' comparison: TDP-43^{Q331K/Q331K} mice that dug consistently well were designated MB+, and those that dug consistently poorly were designated MB- (Fig. 7a,b). We hypothesized that transcriptomic differences between these two genotypically homogeneous groups would indicate molecular pathways that influence the risk of developing cognitive impairment. Using this strategy, we found 410 gene-expression and 61 splicing differences between MB+ and MB- groups (Fig. 7c and Supplementary Fig. 6g,h), which were entirely different from those seen in the earlier comparison with wild-type mice when all eight TDP-43^{Q331K/Q331K} mice were considered as one group (Figs. 4g and 5b). For 78% of these genes, MB+ and MB- mice demonstrated opposing expression changes relative to wild-type (Fig. 7c and Supplementary Tables 1 and 2). Effectively, for these genes, an expression change in one direction is associated with a poor behavioral phenotype yet an expression change in the opposite direction is associated with improved behavior. Furthermore, there was no difference in TDP-43 expression or the degree of TDP-43 gain of function as evidenced by *Sort1* splicing between MB+ and MB- groups. Taken together, these data indicate that the MB +/- comparison genes could be metastable modulators of TDP-43-mediated cognitive dysfunction.

Notably, two of the genes from the MB +/- comparison have previously been linked with suppression of neurodegeneration: *Atxn2* and *Arid4a*. Compared to wild-type mice, MB+ mice demonstrated reduced *Atxn2* expression, while MB- mice demonstrated increased *Atxn2* expression. This is in keeping with previous observations that *Atxn2* knockdown suppresses TDP-43 toxicity in yeast, *Drosophila* and mouse^{31,32}. Furthermore, intermediate expansions of *Atxn2* CAG repeat length are associated with ALS disease risk in humans³¹. Similarly, reduced expression of the chromatin-modeling gene *Arid4a* in MB+ mice is noteworthy, as we previously found that loss-of-function mutations in *hat-trick*, the *Drosophila* ortholog of *Arid4a*, suppress TDP-43-mediated neurodegeneration in flies¹². It is therefore likely that reduced levels of *Atxn2* and *Arid4a* are similarly neuroprotective in TDP-43^{Q331K/Q331K} MB+ mice.

To identify the most significant pathways linked with phenotypic heterogeneity in the MB +/- comparison, we cross-referenced the differential gene expression list with the Gene Ontology database for biological processes (Fig. 7c). Genes downregulated in MB+ mice were enriched for biological processes involving transcription, DNA methylation and chromatin modification. Genes upregulated in MB+ mice were enriched for processes involving protein translation and myelination, including the myelin repair gene *Olig1* and *Mbp*, which encodes myelin basic protein (Supplementary Table 2). Furthermore, examination of the splicing gene list also identified *Mbp* as a candidate (Fig. 7d,e). Specifically, MB- mice demonstrated a significantly increased expression of a specific splice form that is predicted to encode Golli-Mbp, in which three additional exons upstream of classical *Mbp* are normally expressed in nonmyelinating cells, including neurons, and in immature oligodendrocytes³³. Collectively, this Gene Ontology analysis identifies an association between the upregulation of protein translation and oligodendrocyte genes and improved behavior in TDP-43^{Q331K/Q331K} mice, and suggests that the promotion of myelin repair pathways by oligodendrocytes in a mature state contributes to improved cognition.

To confirm the validity of MB +/- hits, we deliberately swapped data from the worst-performing MB+ mouse with that of the

best-performing MB- mouse. This resulted in all transcriptomic hits disappearing from the analysis (Fig. 7f). We also compared only the three best-performing MB+ mice with the three worst-performing MB- mice and found a diminished hit list, but one that largely overlapped with the genes from the complete MB +/- comparison. Furthermore, we found two TDP-43^{Q331K/Q331K} mice that were littermates yet demonstrated contrasting digging behavior on repeated assessment (Fig. 7a,b). This indicated that transcriptomic differences between MB+ and MB- groups were not due to a genetic founder effect in our breeding program. Collectively, these data indicate that the MB +/- transcriptomic differences were genuinely reflective of two phenotypic subsets of young TDP-43^{Q331K/Q331K} mice.

TDP-43^{Q331K} mice demonstrate age-related deterioration of cortical transcriptomes with altered expression and splicing of other ALS-linked genes.

Aging is the greatest known risk factor for sporadic ALS-FTD. To determine the effects of aging on TDP-43^{Q331K} mice, we performed a frontal cortical RNA-seq study in 20-month-old mice (Fig. 8a,b,e,f and Supplementary Fig. 7a,b). Comparison of wild-type and mutant mice revealed transcriptomic differences that partly overlapped with the 5-month-old dataset (Fig. 8c,d,g,h). Aged mutant mice still demonstrated a gain of function of TDP-43, increased retention of *Mapt* exons 2 and 3, and reduced *Nek1* and *Pvalb* expression. However, a broader range of transcriptomic changes was seen, further implicating inhibitory interneuronal disturbances, including downregulation of *Sirt1* and *Ppargc1a*, which encode proteins involved in *Pvalb* transcription, and downregulation of *Gad1* (*Gad67*), which encodes the GABA synthetic protein glutamate decarboxylase (Supplementary Table 1). Aged mice also demonstrated downregulation of *Tbk1* (encoding Tank binding protein kinase 1) (Fig. 8d), loss-of-function mutations of which cause ALS and FTD^{34,35}. Several other ALS-FTD-linked genes also demonstrated significant downregulation, including *Chmp2b*, mutations of which cause FTD³⁶, *Erbp4*, mutations of which cause ALS³⁷, the ALS risk-linked genes *Epha4* and *Kifap338,39*, and the TDP-43 nuclear import factor *Kpnb1*⁴⁰. We also observed altered splicing of ALS-linked genes *Matr3*⁴¹ (decreased exclusion of exon 14, which encodes a zinc finger domain) and *Sqstm1*⁴² (Fig. 8h-j and Supplementary Fig. 7f,g). For *Sqstm1* (encoding sequestosome 1), two splice variants (major and minor) were detected in wild-type and mutant mice, but a third variant was present only in mutants. This TDP-43^{Q331K}-specific variant comprises a truncated exon 7 and a 2-bp frameshift in exon 8, which is predicted to introduce a premature stop codon with loss of the C-terminal ubiquitin-associated domain of sequestosome 1 (Fig. 8j). Furthermore, Gene Ontology and pathway analysis of the RNA-seq dataset in 20-month-old mice revealed many more significant networks than had been identified in 5-month-old TDP-43^{Q331K} mice. Aged mutants demonstrated changes in processes classically linked to neurodegeneration, including protein ubiquitination, autophagy and glutamate receptor activity, while KEGG (Kyoto Encyclopedia of Genes and Genomes) pathway analysis highlighted "ALS" and immune pathways (Fig. 8b). These pathways were not invoked in young mice (Fig. 4g). Collectively, these observations in aged mutant mice validate key transcriptomic findings in young mutants, link aberrant TDP-43 homeostasis with other key ALS-FTD-linked genes, and indicate age-related progressive changes in the cortical transcriptomes of TDP-43^{Q331K} mice.

Finally, to identify transcriptomic differences associated with long-term resistance to cognitive impairment, we performed an MB +/- comparison in aged mice. As most aged TDP-43^{Q331K/Q331K} mice had progressed to an MB- state by 20 months, we compared TDP-43^{Q331K/+} mice, which we were able to stratify into MB+ and MB- groups. This comparison yielded only 21 differentially expressed genes and 45 splicing differences between TDP-43^{Q331K/+} MB+ and MB- mice, which did not overlap with those genes iden-

tified in the MB +/- comparison of 5-month-old TDP-43^{Q331K/Q331K} mice (Supplementary Fig. 7c–e). This suggests that aged TDP-43^{Q331K/+} mice are not amenable to stratification in the same way as young TDP-43^{Q331K/Q331K} mice, and further suggests that modulation of MB +/- genes early in life has the potential to influence longer-term susceptibility to cognitive impairment secondary to aberrant TDP-43 homeostasis.

Discussion

Here we show that with a single human disease-linked base change in murine *Tardbp* it is possible to replicate behavioral, pathological and transcriptomic features of the ALS-FTD spectrum. By creating a model that mimics the human mutant state as closely as possible and in the absence of exogenous expression, we determined that the Q331K mutation perturbs TDP-43 autoregulation. This leads to an increase in TDP-43 expression (effectively a gain-of-function defect). Notably, spinal cords from sporadic ALS patients and from *TARDBP* mutation carriers demonstrate increased TDP-43 mRNA expression, as do human stem-cell-derived motor neurons with *TARDBP* mutations^{43,44}. This indicates that TDP-43 misregulation could underpin the human disease state.

Lumbar motor neurons of TDP-43^{Q331K/Q331K} mice demonstrated upregulation of genes that may confer neuroprotection and did not demonstrate TDP-43 misregulation, both of which might explain why mutant mice did not demonstrate significant neuromuscular phenotypes. By contrast, the FTD-like phenotypes in mutant mice were more marked. The identification of reduced parvalbumin expression as a possible cause for cognitive impairment in ALS-FTD is intriguing, as parvalbumin interneuron loss has been observed in sporadic ALS and FTD²⁶. As parvalbumin interneurons are GABAergic, a reduction in their numbers could increase activity of cortical projection neurons, with excitotoxic consequences. Early interneuronal dysfunction may have analogous consequences in the spinal cord and is suggested by our observation that TDP-43 autoregulation is perturbed in the spinal cord, but not in motor neurons.

That TDP-43^{Q331K} mice demonstrate a specific increase in inclusion of *Mapt* exons 2 and 3 is of great interest, as oligomers of the 2N splice isoform of tau appear to have a greater ability to provoke tau aggregation than 0N and 1N isoforms³⁰, and inclusion of exons 2 and 3 influences subcellular localization and protein–protein interactions of tau⁴⁵. Furthermore, in humans the H2 *Mapt* haplotype is associated with a greater inclusion of *Mapt* exon 3 and is associated with an earlier age of onset in FTD^{46,47}. Although we did not observe clear disturbances of total tau localization in TDP-43^{Q331K} mice, more detailed analyses to identify specific tau isoforms are warranted. Our identification of a mechanistic link between TDP-43 and *Mapt* adds to growing evidence that ALS-FTD is characterized by both TDP-43 and tau pathology⁴⁸. Furthermore, transcriptomic analysis of aged TDP-43^{Q331K} mice elucidated changes in other ALS-FTD linked genes. Collectively, these findings emphasize a central role for TDP-43 in neurodegeneration.

Finally, we observed phenotypic heterogeneity among mutant mice with the same genotype and identified distinct transcriptomic profiles corresponding to differing phenotypes. This transcriptomic dataset contains genes already implicated in neurodegeneration, including *Arid4a*¹² and *Atnx2*³¹. The unbiased discovery of *Atnx2* downregulation as a hit in our model is consistent with observations validating *Atnx2* knockdown as a therapeutic approach for ALS-FTD³². Our data suggest a delicate balance in the transcriptome of the brain, which is metastable and can influence disease onset or progression. Identifying the environmental factors that influence this balance is a priority in future studies. Indeed, the strong representation of DNA methylation and chromatin modeling genes in the MB +/- comparison suggests a critical role for epigenetic influences in determining disease susceptibility. Genes with roles in protein translation and oligodendrocyte biology, including myelina-

tion, also featured in our list of putative disease modifiers, and it is encouraging that both these pathways have roles in neurodegenerative disease^{49,50}. Our wider list of potential modifiers of disease is composed of over 450 gene-expression and splicing changes that are associated with improved behavior in TDP-43^{Q331K/Q331K} mice. We conclude that this list contains additional suppressors of neurodegeneration that will help direct efforts toward developing treatments for ALS-FTD.

Methods

Methods, including statements of data availability and any associated accession codes and references, are available at <https://doi.org/10.1038/s41593-018-0113-5>.

Received: 4 August 2017; Accepted: 15 January 2018;

Published online: 19 March 2018

References

- Burrell, J. R. et al. The frontotemporal dementia-motor neuron disease continuum. *Lancet* **388**, 919–931 (2016).
- Neumann, M. et al. Ubiquitinated TDP-43 in frontotemporal lobar degeneration and amyotrophic lateral sclerosis. *Science* **314**, 130–133 (2006).
- Arai, T. et al. TDP-43 is a component of ubiquitin-positive tau-negative inclusions in frontotemporal lobar degeneration and amyotrophic lateral sclerosis. *Biochem. Biophys. Res. Commun.* **351**, 602–611 (2006).
- Sreedharan, J. et al. TDP-43 mutations in familial and sporadic amyotrophic lateral sclerosis. *Science* **319**, 1668–1672 (2008).
- Benajiba, L. et al. *TARDBP* mutations in motoneuron disease with frontotemporal lobar degeneration. *Ann. Neurol.* **65**, 470–473 (2009).
- Tollervey, J. R. et al. Characterizing the RNA targets and position-dependent splicing regulation by TDP-43. *Nat. Neurosci.* **14**, 452–458 (2011).
- Ayala, Y. M. et al. TDP-43 regulates its mRNA levels through a negative feedback loop. *EMBO J* **30**, 277–288 (2011).
- Philips, T. & Rothstein, J. D. Rodent models of amyotrophic lateral sclerosis. *Curr. Protoc. Pharmacol.* **69**, 5.67, <https://doi.org/10.1002/0471141755.ph0567s69> (2015).
- Arnold, E. S. et al. ALS-linked TDP-43 mutations produce aberrant RNA splicing and adult-onset motor neuron disease without aggregation or loss of nuclear TDP-43. *Proc. Natl Acad. Sci. USA* **110**, E736–E745 (2013).
- Wu, L. S. et al. TDP-43, a neuro-pathogenesis factor, is essential for early mouse embryogenesis. *Genesis* **48**, 56–62 (2010).
- Buratti, E. Functional significance of TDP-43 mutations in disease. *Adv. Genet.* **91**, 1–53 (2015).
- Sreedharan, J., Neukomm, L. J., Brown, R. H. Jr. & Freeman, M. R. Age-dependent TDP-43-mediated motor neuron degeneration requires GSK3, hat-trick, and xmas-2. *Curr. Biol.* **25**, 2130–2136 (2015).
- Johnson, B. S. et al. TDP-43 is intrinsically aggregation-prone, and amyotrophic lateral sclerosis-linked mutations accelerate aggregation and increase toxicity. *J. Biol. Chem.* **284**, 20329–20339 (2009).
- Jhuang, H. et al. Automated home-cage behavioural phenotyping of mice. *Nat. Commun.* **1**, 68 (2010).
- Borghero, G. et al. Genetic architecture of ALS in Sardinia. *Neurobiol. Aging* **35**, 2882.e2887–2882.e2812 (2014).
- Ahmed, R. M. et al. Assessment of eating behavior disturbance and associated neural networks in frontotemporal dementia. *JAMA Neurol.* **73**, 282–290 (2016).
- Burden, S. J., Yumoto, N. & Zhang, W. The role of MuSK in synapse formation and neuromuscular disease. *Cold Spring Harb. Perspect. Biol.* **5**, a009167 (2013).
- Berger, R. et al. Analysis of aldehyde oxidase and xanthine dehydrogenase/oxidase as possible candidate genes for autosomal recessive familial amyotrophic lateral sclerosis. *Somat. Cell Mol. Genet.* **21**, 121–131 (1995).
- Garattini, E., Fratelli, M. & Terao, M. The mammalian aldehyde oxidase gene family. *Hum. Genomics* **4**, 119–130 (2009).
- Jiang, Y. M. et al. Gene expression profile of spinal motor neurons in sporadic amyotrophic lateral sclerosis. *Ann. Neurol.* **57**, 236–251 (2005).
- Kolarcik, C. L. & Bowser, R. Retinoid signaling alterations in amyotrophic lateral sclerosis. *Am. J. Neurodegener. Dis.* **1**, 130–145 (2012).
- Mar, A. C. et al. The touchscreen operant platform for assessing executive function in rats and mice. *Nat. Protoc.* **8**, 1985–2005 (2013).
- Thomas, A. et al. Marble burying reflects a repetitive and perseverative behavior more than novelty-induced anxiety. *Psychopharmacology (Berl.)* **204**, 361–373 (2009).
- Kenna, K. P. et al. NEK1 variants confer susceptibility to amyotrophic lateral sclerosis. *Nat. Genet.* **48**, 1037–1042 (2016).

25. Brenner, D. et al. *NEK1* mutations in familial amyotrophic lateral sclerosis. *Brain* **139**, e28 (2016).
26. Nihei, K., McKee, A. C. & Kowall, N. W. Patterns of neuronal degeneration in the motor cortex of amyotrophic lateral sclerosis patients. *Acta Neuropathol.* **86**, 55–64 (1993).
27. Kim, H., Åhrlund-Richter, S., Wang, X., Deisseroth, K. & Carlén, M. Prefrontal parvalbumin neurons in control of attention. *Cell* **164**, 208–218 (2016).
28. Polymenidou, M. et al. Long pre-mRNA depletion and RNA missplicing contribute to neuronal vulnerability from loss of TDP-43. *Nat. Neurosci.* **14**, 459–468 (2011).
29. Hutton, M. et al. Association of missense and 5'-splice-site mutations in tau with the inherited dementia FTDP-17. *Nature* **393**, 702–705 (1998).
30. Swanson, E. et al. Extracellular tau oligomers induce invasion of endogenous tau into the somatodendritic compartment and axonal transport dysfunction. *J. Alzheimers Dis.* **58**, 803–820 (2017).
31. Elden, A. C. et al. Ataxin-2 intermediate-length polyglutamine expansions are associated with increased risk for ALS. *Nature* **466**, 1069–1075 (2010).
32. Becker, L. A. et al. Therapeutic reduction of ataxin-2 extends lifespan and reduces pathology in TDP-43 mice. *Nature* **544**, 367–371 (2017).
33. Harauz, G. & Boggs, J. M. Myelin management by the 18.5-kDa and 21.5-kDa classic myelin basic protein isoforms. *J. Neurochem.* **125**, 334–361 (2013).
34. Freischmidt, A. et al. Haploinsufficiency of TBK1 causes familial ALS and fronto-temporal dementia. *Nat. Neurosci.* **18**, 631–636 (2015).
35. Cirulli, E. T. et al. Exome sequencing in amyotrophic lateral sclerosis identifies risk genes and pathways. *Science* **347**, 1436–1441 (2015).
36. Skibinski, G. et al. Mutations in the endosomal ESCRTIII-complex subunit CHMP2B in frontotemporal dementia. *Nat. Genet.* **37**, 806–808 (2005).
37. Takahashi, Y. et al. *ERBB4* mutations that disrupt the neuregulin-ErbB4 pathway cause amyotrophic lateral sclerosis type 19. *Am. J. Hum. Genet.* **93**, 900–905 (2013).
38. Van Hoecke, A. et al. *EPHA4* is a disease modifier of amyotrophic lateral sclerosis in animal models and in humans. *Nat. Med.* **18**, 1418–1422 (2012).
39. Landers, J. E. et al. Reduced expression of the Kinesin-Associated Protein 3 (*KIFAP3*) gene increases survival in sporadic amyotrophic lateral sclerosis. *Proc. Natl Acad. Sci. USA* <https://doi.org/10.1073/pnas.0812937106> (2009).
40. Nishimura, A. L. et al. Nuclear import impairment causes cytoplasmic trans-activation response DNA-binding protein accumulation and is associated with frontotemporal lobar degeneration. *Brain* **133**, 1763–1771 (2010).
41. Johnson, J. O. et al. Mutations in the Matrin 3 gene cause familial amyotrophic lateral sclerosis. *Nat. Neurosci.* **17**, 664–666 (2014).
42. Fecto, F. et al. *SQSTM1* mutations in familial and sporadic amyotrophic lateral sclerosis. *Arch. Neurol.* **68**, 1440–1446 (2011).
43. Koyama, A. et al. Increased cytoplasmic TARDBP mRNA in affected spinal motor neurons in ALS caused by abnormal autoregulation of TDP-43. *Nucleic Acids Res.* **44**, 5820–5836 (2016).
44. Egawa, N. et al. Drug screening for ALS using patient-specific induced pluripotent stem cells. *Sci. Transl. Med.* **4**, 145ra104 (2012).
45. Liu, C., Song, X., Nisbet, R. & Götz, J. Co-immunoprecipitation with tau isoform-specific antibodies reveals distinct protein interactions and highlights a putative role for 2N tau in disease. *J. Biol. Chem.* **291**, 8173–8188 (2016).
46. Trabzuni, D. et al. MAPT expression and splicing is differentially regulated by brain region: relation to genotype and implication for tauopathies. *Hum. Mol. Genet.* **21**, 4094–4103 (2012).
47. Borroni, B. et al. Association between tau H2 haplotype and age at onset in frontotemporal dementia. *Arch. Neurol.* **62**, 1419–1422 (2005).
48. Behrouzi, R. et al. Pathological tau deposition in motor neurone disease and frontotemporal lobar degeneration associated with TDP-43 proteinopathy. *Acta Neuropathol. Commun.* **4**, 33 (2016).
49. Moreno, J. A. et al. Oral treatment targeting the unfolded protein response prevents neurodegeneration and clinical disease in prion-infected mice. *Sci. Transl. Med.* **5**, 206ra138 (2013).
50. Kang, S. H. et al. Degeneration and impaired regeneration of gray matter oligodendrocytes in amyotrophic lateral sclerosis. *Nat. Neurosci.* **16**, 571–579 (2013).

Acknowledgements

We thank Babraham Institute Experimental Unit staff for technical assistance, A. Weiss for technical assistance at UMMS, M. Brodsky for assistance with CRISPR mutagenesis, the DERC morphology core at UMMS for assistance with histological preparations, and S. Hilton for assistance with OR testing. We thank members of M.P.C.'s laboratory and J.-M. Gallo for discussions. E.K. is supported by a grant from the Korean Health Technology R&D Project, Korea-UK AD Collaborative Project (HI14C2173), Ministry of Health and Welfare, Republic of Korea. R.A. is supported by MRC grant MR/L003813/1. S.Y. is supported by an ARUK grant (RF-2016A-1). M.P.C. is supported by the van Geest Foundation. R.H.B. gratefully acknowledges support from the ALS Association, Project ALS, Target ALS, ALS-One, ALS Finding A Cure, the Max Rosenfeld fund for ALS Research, and NIH grants RO1NS088689, RO1FD004127, RO1NS065847 and RO1 NS073873. J. Sreedharan is funded by the Motor Neuron Disease Association, the Medical Research Council UK, the Lady Edith Wolfson Fellowship Fund, and the van Geest Foundation.

Author contributions

J. Sreedharan, M.A.W., M.P.C., R.H.B., T.J.B., J.F., R.M. and L.M.S. designed experiments. M.A.W. and J. Sreedharan performed studies on cohort 1 mice including behavioral assessments, histology and transcriptomics. E.K. performed touchscreen studies on cohort 2 mice with assistance from B.U.P. A.D. collated ACBM data and quantified NMJ innervation. R.A. performed spinal cord dissections for laser capture and histology. O.M.P. and J.M. conducted histological studies and image analysis. J. Stephenson performed motor behavioral studies. S.Y. and E.K. performed the OR assay. F.M. quantified motor neurons and western blots. Z.L. performed sequencing to exclude off-target mutagenesis events. S.A. and A.S.-P. assisted with analysis of RNA-seq data and statistical analyses, respectively. R.R.R. performed neuromuscular electrophysiological studies. Y.B. and T.S. developed ACBM software and analyzed ACBM data. J. Sreedharan wrote the manuscript with contributions from all authors.

Competing interests

The authors declare no competing interests.

Additional information

Supplementary information is available for this paper at <https://doi.org/10.1038/s41593-018-0113-5>.

Reprints and permissions information is available at www.nature.com/reprints.

Correspondence and requests for materials should be addressed to J.S.

Publisher's note: Springer Nature remains neutral with regard to jurisdictional claims in published maps and institutional affiliations.

Methods

CRISPR/Cas9 mutagenesis to introduce the Q331K mutation. Nucleases were designed to be close to or overlap the desired point mutation. Three CRISPR/Cas9 nucleases were tested for activity using a GFP reporter plasmid. A 121-bp single-stranded DNA oligonucleotide with the point mutation at the midpoint was used as a repair template. Guide RNA (gRNA) and a capped Cas9 mRNA were synthesized and injected with the donor oligonucleotide into 270 single-cell C57Bl/6J embryos. For sequences see Supplementary Table 3. Off-targets were predicted using CRISPRseek³¹.

Mouse breeding and maintenance. Mouse founder number 52 was outcrossed with wild-type C57Bl/6J mice through to the F₃ generation. Three F₃ male siblings were bred to wild-type C57Bl/6J mice to generate F₁ TDP-43^{Q331K/+} mutants, which were intercrossed to generate animals for study.

Power calculations were based on historical Rotarod and touchscreen data of wild-type mice. This indicated required group sizes of 15 animals per genotype to identify a ~20% difference in performance between genotypes. Animals were only excluded from analyses if specified in the following methods.

Mouse breeding was carried out in the UK and USA. ACBM was carried out at the Brown University Rodent Neurodevelopment Behavior Testing Facility. All procedures were approved by the Brown University Animal Care and Use Committee. Touchscreen analysis, marble burying, object recognition, motor behavior, food intake and weight measurement, pathology, electrophysiology and RNA sequencing all took place in the UK. All experiments were conducted in accordance with the United Kingdom Animals (Scientific Procedures) Act (1986) and the United Kingdom Animals (Scientific Procedures) Act (1986) Amendment Regulations 2012. Animals were housed in cages of up to five animals under a 12 h light/dark cycle.

Genotyping. The Q331K mutation coincidentally introduces a SapI/EarI restriction site, which facilitates genotyping (see Supplementary Table 4).

Automated continuous behavioral monitoring. Ten TDP43^{Q331K/Q331K} and 10 wild-type animals (5 female, 5 male of each genotype) from the same breeding campaign were obtained from the animal care facility at the University of Massachusetts Medical School. Animals were group housed between sessions, but housed individually during the 5-day ACBM recording sessions. Cages were monitored with a Firefly MV 0.3 MP Mono FireWire 1394a (Micron MT9V022) at 30 frames/s. Cameras were connected to a workstation with Ubuntu 14.04 using a Firewire card to connect to all cameras. For processing by the computer vision system, all videos were downsampled to 320 × 240 pixels.

The system used for ACBM was modified from that previously described and was reimplemented in Python and NVIDIA's CUDNN to speed video analysis subroutines. All video analyses were conducted using the Brown University high-performance computer cluster. The system was retrained using data collected at the Brown Rodent Neuro-Developmental Behavior Testing facility (~20 h of video and 40 animals total). Data were annotated by hand for eight behaviors as previously described (drink, eat, groom, hang, rear, rest, sniff, walk). Accuracy was evaluated using cross-validation. The average agreement with human annotations was 78% for individual behavior and 83% overall for individual frames. Evaluation of the system was also run on a subset of the data collected for the present study, which found an overall mean agreement of 71% for individual behaviors and 82% over all video frames.

Rotarod. Motor testing was performed using a Rotarod (Ugo Basile, model 7650, Varese, Italy). At least 24 h before testing, mice were first trained for 5 min at the slowest speed and then 7 min with acceleration. During testing mice were subjected to 7-min trials with acceleration from 3.5 to 35 r.p.m. In each session mice were tested three times with a trial separation of 30 min. The latency to fall (maximum 420 s) for each mouse was recorded and mean values for each mouse calculated. An individual mouse recording was excluded if the mouse fell off the rod while moving backwards, accidentally slipped or jumped off at slow speed. Two consecutive passive rotations were counted as a fall and the time recorded as the end point for that mouse. Mouse weights were recorded immediately after completion of Rotarod testing. All testing was conducted by operators who were blind to genotype and in a randomized order.

Feeding. Cages containing either two or three mice of the same genotype were supplied with 400 g of food on Monday mornings. The following Monday the surplus food in the hopper, together with any obvious lumps of food in the cage, was removed and weighed. The difference from 400 g was calculated and recorded as the total food consumed in 7 d. This was divided by the number of mice in a given cage. Weekly consumption was calculated for 9 consecutive weeks. Mice were 12 months of age when recording commenced. All testing was conducted while blind to genotype and in a randomized order.

Touchscreen studies. 48 male mice ($n = 16$ per genotype) were housed in groups of 2–5 per cage under a 12-h light/dark cycle (lights on at 7:00 pm). Testing was conducted during the dark phase. To ensure sufficient motivation, animals were

food-restricted to ~85–90% of free-fed weights by daily provision of standard laboratory chow pellets (RM 3; Special Diet Services, Essex, UK). Drinking water was available ad libitum.

Experiments were performed in standard mouse Bussey–Saksida touchscreen chambers (Campden Instruments Ltd, Loughborough, UK). The reward for each correct trial was delivery of 20 μ L of milkshake (Yazoo strawberry milkshake; FrieslandCampina UK, Horsham, UK). The chambers are equipped with infrared activity beams (rear beam 3 cm from magazine port and front beam 6 cm from screen) to monitor locomotor activity.

Following 2 d of habituation to touchscreen chambers, mice underwent pretraining and training. Briefly, mice were first trained to touch the correctly lit stimulus in return for a food reward, and to initiate a trial by poking and removing their nose from the magazine. Finally, mice were discouraged from making responses at unilluminated apertures by a 5 s time-out period during which the chamber was illuminated. Investigators were blind to genotype.

Five-choice serial reaction time task (5-CSRTT). Upon completion of training at 2 s stimulus duration (baseline), mice were tested in 4 sessions of decreasing stimulus durations (2.0 s, 1.5 s, 1.0 s, 0.5 s) pseudorandomly within a session. Animals that had not reached the criterion (> 80% accuracy, < 20% omissions in two consecutive sessions in baseline training before entering the probe test, $n = 1$ in the first probe test) or whose body weights were below 80% of free-feeding weight ($n = 1$ in the first and $n = 1$ in the second probe test) were excluded.

Fixed-ratio (FR) and progressive-ratio (PR) schedule. FR and PR studies were conducted as described elsewhere⁵². When performance stabilized on FR5 (completion of 30 trials within 20 min), all mice were tested on two sessions of an unrestricted FR5, which allowed an unlimited number of trials in 60 min. Next, animals underwent three sessions of PR4, in which animals need to make a progressively increasing number of responses (i.e. 1, 5, 9, 13, ...) in each subsequent trial to obtain a single reward. PR session terminated after either 60 min or 5 min of inactivity. Breakpoint, the number of responses made to obtain the reward in the last completed trial, was recorded as an index of motivation.

Object recognition. The novel object recognition task was conducted as described elsewhere⁵³ in a randomized order with the operator blind to genotype and under dimmed white light. Six-month-old male mice ($n = 8$ or 9 per genotype) were randomly chosen from cohort 2. Mice were habituated to a Y-maze for 5 min. One day later mice were reintroduced to the Y-maze, which now contained two identical objects in each arm. Exploration time for each object over a 5 min period was recorded (sample phase). Mice were then removed from the maze and one of the objects replaced with a novel object. After a delay of 1 min or 3 h mice were reintroduced to the maze (choice phase) and the time spent exploring each object over a 5 min period was recorded. The memory for the familiar object was expressed as a discrimination ratio (difference in exploration of the novel and familiar objects divided by the total object exploration time).

Marble burying. All testing was conducted in the morning and blind to genotype. Cages of size 39.1 cm × 19.9 cm × 16.0 cm height (Tecniplast) were used. Fresh bedding material (Datesand, grade 6) was placed into each cage to a height of ~6 cm. Ten glass marbles (1 cm) were placed evenly across the bedding. Ten cages were prepared in a single round. One mouse was placed in each of the cages and the lids replaced. Mice were left undisturbed for 30 min under white light. Mice were then removed and the number of marbles buried by at least two-thirds was scored. Cages were reset using the same bedding material to test another ten mice. In stratifying mice before frontal cortical RNA-seq, animals were tested twice, 3 d apart, to identify those that consistently buried high or low numbers of marbles.

Repeat behavioral studies. Cohort 1 mice underwent Rotarod, weight, feeding and marble testing all under a standard light/dark cycle (lights on at 7:00 am for 12 h). Cohort 2 mice underwent all touchscreen, object recognition and Rotarod studies under a reverse light/dark cycle.

Pathology studies. Mice were killed by cervical dislocation and tissues were processed as follows.

Brains. Right hemispheres were processed for RNA and/or protein extraction (see below). Left hemispheres were immersion-fixed in 4% paraformaldehyde (PFA) at 4 °C for 24 h, washed in PBS, cryoprotected in 30% sucrose in PBS at 4 °C, embedded and frozen in M1 matrix (Thermo Fisher Scientific) on dry ice and sectioned coronally at 16 μ m thickness on a cryostat (Leica Biosystems). Sections were mounted on Superfrost Plus charged slides (Thermo Fisher Scientific), allowed to dry overnight and stored at –80 °C.

Spinal cords. Vertebral columns were dissected, immersion-fixed in 4% PFA at 4 °C for 48 h, washed in PBS and dissected to extract spinal cords and nerve roots. The lumbar enlargement was subdissected, cryoprotected in 30% sucrose at 4 °C, embedded in M1 matrix in a silicon mold, frozen on dry ice and sectioned at 16 μ m thickness onto charged slides, briefly air dried and stored at –80 °C.

Antigen retrieval and immunostaining. Sections were thawed at room temperature and briefly rinsed in distilled water. Antigen retrieval was performed by heating slides for 20 min at 95 °C in antigen unmasking solution, Tris-based (Vector Laboratories). Sections were cooled to room temperature, washed in distilled water, and blocked and permeabilized in a solution containing 5% bovine serum albumin (BSA), 0.1% Triton X-100 and 5% serum (specific to secondary antibody species used) for 1 h at room temperature. Slides were incubated with primary antibody for 2 h at room temperature or 4 °C overnight in fivefold-diluted blocking buffer. Secondary antibodies were applied for 1 h at room temperature (Alexa Fluor conjugated, Thermo Fisher Scientific; 1:500 in diluted block). Sections were counterstained and mounted with Vectashield hardset with DAPI (Vector Labs). Alexa Fluor 568 conjugated secondary antibodies were false-colored magenta (ImageJ 1.15j).

To quantify parvalbumin-positive neurons, parvalbumin-stained sections were imaged on a Nikon Ti-E live cell imager. Images were acquired using a Plan Apo lambda 10× objective with a final image dimension of 4,608 × 4,608 with 2 × 2 binning, stitched (NIS-Elements) and analyzed (ImageJ 1.15j) blind to genotype. For each mouse, matching sections through the frontal cortex from bregma 2.8 mm to 0.74 mm were analyzed, with a total of 10 sections per mouse quantified for 3 wild-type and 3 TDP43^{Q331K/Q331K} mice. Images were converted to grayscale and thresholded to produce a binary image. Consistent regions of interest were drawn around the cortex using the polygon selection tool and the 'analyze particle' function was used to count cells.

To investigate TDP-43 in parvalbumin-positive neurons, sections were co-stained with antibodies against TDP-43 and parvalbumin and imaged using a Zeiss LSM 780, AxioObserver with a Plan-Apochromat 63×/1.40 Oil DIC M27 objective running Zen system software. Data analysis (ImageJ 1.15j) and imaging was carried out blind to genotype. For each cell, a maximum intensity projection of z stacks was created and regions of interest were drawn around the nucleus and the cytoplasm using the polygon selection tool. Area, integrated density and mean gray value measurements were taken for the cytoplasm and nucleus, together with a background reading. Corrected total fluorescence for a region of interest was calculated as follows:

$$\text{CTF} = \text{integrated density} - (\text{area region of interest} \times \text{background fluorescence})$$

Corrected fluorescence was recorded for at least 10 cells per mouse in matched sections corresponding to bregma 1.18 mm.

To quantify AOX1 fluorescence in lumbar motor neurons, sections were co-stained with antibodies against AOX1 and neurofilament heavy chain and imaged on a Nikon Ti-E live cell imager with a Plan Apo VC 20× DIC N2 objective with a final image dimension of 1,024 × 1,024 pixels and 2 × 2 binning. Data analysis (ImageJ 1.15j) and imaging were carried out blind to genotype. Corrected fluorescence was recorded for at least 29 cells per mouse.

TDP-43 immunostaining in spinal cord and brain were imaged using a Nikon Ti-E live cell imager and a Plan Apo VC 100× Oil objective with a final image dimension of 1,024 × 1,024 pixels and 2 × 2 binning. Images are a maximum intensity z stack created using ImageJ 1.15j with a z step of 0.2 μm.

Tau immunostaining in cortex was imaged using a Zeiss LSM 780, AxioObserver with a Plan-Apochromat 63×/1.40 Oil DIC M27 objective running Zen system software. Images are a maximum intensity z stack created using ImageJ 1.15j.

For list of primary antibodies, see Supplementary Table 5.

Nissl staining of spinal cord and brain. Sections were thawed at room temperature, washed in distilled water, stained with cresyl etch violet (Abcam) for 5 min, briefly washed in distilled water, dehydrated in 100% ethanol, cleared in xylene, mounted (Permount, Fisher) and dried overnight at room temperature. Images were taken on a Zeiss Axio Observer.Z1 running Axiovision SE64 release 4.8.3 software. Cortical images were taken with an EC Plan-Neofluar 5×/0.16 M27 objective with a total area of 4,020 × 2,277 pixels autostitched in the software. Spinal cord images were acquired with an LD Plan-Neofluar 20×/0.4 corr M27 objective with an image size of 1,388 × 1,040 pixels.

Lumbar spinal motor neuron quantification. Motor neurons were quantified as described elsewhere⁵⁴. Briefly, large motor neurons (diameter > 20 μm) in the ventral horn were counted blind to genotype in 18 sections from the lumbar L3–5 levels of each animal.

Cellular quantification in brain. Data analysis using ImageJ 1.15j and imaging was carried out blind to genotype. For total frontal cortical area, matching sections through the frontal cortex from bregma 2.8 mm to 0.74 mm were selected with a total of ten sections quantified for six wild-type and six TDP43^{Q331K/Q331K} mice. Matching regions of interest were drawn around the cortex and the area quantified using the 'measure' function. To count cells in cortical subregions, matching sections based on bregma references were identified. Images were converted to grayscale and thresholded to produce a binary image. Consistent regions of interest were drawn around the cortex and the 'analyze particle' function used to count cells. A minimum size of 10 pixels ensured that intact cells were counted and results were displayed with the overlay option selected.

Western blotting. Brain tissues were weighed to ensure equal amounts of starting material between samples, thawed on ice and processed using a modified fractionation protocol⁵⁵. Briefly, tissue was sequentially homogenized and centrifuged using buffers A (NaCl 150 mM, HEPES (pH 7.4) 50 mM, digitonin (Sigma, D141) 25 μg/mL, hexylene glycol (Sigma, 112100) 1 M, protease inhibitor cocktail (Sigma, P8340) 1% v-v) and B (same as buffer A except Igepal (Sigma, I7771) 1% v-v is used in place of digitonin) to extract cytoplasmic and membrane fractions, respectively. The subsequent pellet was sonicated in 1% sarkosyl buffer containing 10 μM Tris-Cl (pH 7.5), 10 μM EDTA, 1 M NaCl and centrifuged (14,000 g for 30 min at 4 °C). The supernatant was taken as the nuclear fraction. Protein lysates were quantified (bicinchoninic acid protein assay, Pierce), electrophoresed in 4–12% or 12% SDS polyacrylamide gels, wet transferred to PVDF membranes, blocked with a 50:50 mixture of Odyssey PBS blocking buffer and PBS with 0.1% Tween-20 for 1 h at room temperature and then probed with primary antibodies at 4 °C overnight. Secondary antibodies were either fluorescently tagged for Odyssey imaging or HRP-tagged for ECL visualization. Western blot band intensities were quantified using Fiji (ImageJ; Version 2.0.0-rc-54/1.51 h; Build: 26f53ffab) using the programs gel analysis menu option in 8-bit grayscale. Quantification was carried out by an independent user blind to genotype. For list of primary antibodies, see Supplementary Table 5.

Muscle histology. The right gastrocnemius was dissected, fixed in 4% PFA at room temperature, washed in PBS for 10 min twice and cryoprotected and stored in 30% sucrose with 0.1% azide. Tissues were placed in a silicone mold with M1 matrix and frozen on dry ice. Longitudinal cryosections (50 μm) were mounted on slides (SuperFrost Plus), air dried at room temperature for 5 min and stored at –80 °C.

To stain neuromuscular junctions (NMJs), slides were brought up to room temperature and incubated in blocking solution (2% BSA, 0.2% Triton X-100, 0.1% sodium azide) for 1 h. Primary antibodies against βIII-tubulin (rabbit polyclonal, Sigma T2200) and synaptophysin (mouse monoclonal, Abcam ab8049) were applied at 1:200 dilution in blocking solution. Sections were incubated at room temperature overnight. Sections were washed in PBS three times and incubated for 90 min with mouse and rabbit Alexa488-conjugated secondary antibodies (Thermo Fisher Scientific) diluted 1:500 in blocking solution together with TRITC-conjugated α-bungarotoxin (Sigma, T0195) 10 μg/ml. Sections were washed in PBS and coverslipped (Vectashield hardset). Confocal z stacks were obtained using a Zeiss LSM 780 AxioObserver with a Plan-Apochromat 20×/0.8 M27 objective running Zen system software; the observer was blind to genotype.

For succinate dehydrogenase (SDH) staining, the left gastrocnemius was dissected, flash frozen in isopentane in liquid nitrogen and stored at –80 °C until use. Frozen sections of 12 μm were prepared and stained using a modified version of a previously described method⁵⁶. Briefly, sections were stained with freshly prepared SDH staining solution at 37 °C for 3 min, washed through saline, acetone and ethanol solutions, cleared in xylene and mounted (Permount). Images were taken using an Olympus BX41 light microscope (10× objective) with Q Capture Pro 6.0.

Quantification of NMJ innervation. NMJs from flattened z stacks of muscle were analyzed (ImageJ; Version 2.0.0-rc-54/1.51 h, build 26f53ffab) blind to genotype. Brightness and contrast thresholds were set to optimize the signal-to-noise ratio of the presynaptic staining (anti-tubulin and anti-synaptophysin). Innervated NMJs were defined as having observed overlap of staining for pre- and postsynaptic elements. Denervated NMJs were defined as α-bungarotoxin signal in the absence of presynaptic staining. A small percentage (~5% in each genotype) of NMJs could not be scored and were excluded from this analysis.

Neuromuscular electrophysiology. Isolated FDB–tibial nerve preparations were mounted in an organ bath in HEPES-buffered MPS of the following composition (mM): Na⁺ (158), K⁺ (5), Ca²⁺ (2), Mg²⁺ (1), Cl⁻ (169), glucose (5), HEPES (5), pH 7.2–7.4, and bubbled with air or 100% O₂ for at least 20 min. The distal tendons were pinned to the base of a Sylgard-lined recording chamber and the proximal tendon connected by 6/0 silk suture to an MLT0202 force transducer (AD Instruments, Oxford, UK). The tibial nerve was aspirated into a glass suction electrode and stimuli (0.1–0.2 ms duration, nominally up to 10 V) were delivered via a DS2 stimulator (Digitimer, Welwyn Garden City, UK) triggered and gated by an AD Instruments Powerlab 26 T interface. Force recordings were captured and digitized at 1 kHz using the Powerlab interface and measured using Scope 4 and Labchart 7 software (AD Instruments) running on PC or Macintosh computers. For motor unit recordings, the stimulating voltage was carefully graded from threshold to saturation to evoke the maximum number of steps in the twitch tension record. Motor unit number estimation was performed by inspection, counting the number of reproducible tensions steps, and by extrapolation between the average twitch tension of the four lowest threshold motor units and the maximum twitch tension. For tetanic stimulation, trains of stimuli 1–5 s in duration were delivered at frequencies of 2–50 Hz. To measure muscle fatigue, 50 Hz stimulus trains 1 s in duration were delivered every 5 s for about a minute. A fatigue index was calculated as the time constant of the best fitting single exponential to the decline of the maximum tetanic force.

Brain RNA isolation. Frontal cortices and hippocampi were subdivided in RNase-free conditions (RNaseZap, Sigma Aldrich) from right hemispheres of freshly killed mice and flash frozen until further use. For RNA extraction, tissue was thawed directly in TRIreagent (Bioline) and RNA isolated following manufacturer's instructions. RNA was purified (RNeasy kit, Qiagen) with on-column DNase treatment and analyzed on an Agilent 2100 Bioanalyzer.

Spinal motor neuron laser capture microdissection. Mice were killed by cervical dislocation. Lumbar spinal cord was rapidly dissected taking care to avoid RNase exposure, embedded in precooled M1 embedding matrix (Thermo) in a silicone mold and flash frozen in isopentane on dry ice. Samples were stored at -80°C until use. Transverse cryosections ($14\ \mu\text{m}$) were taken through the lumbar enlargement and placed onto PEN membrane glass slides (Zeiss) that were kept at -20°C during sectioning. One spinal cord was processed at a time. Approximately 50 sections were taken per mouse and placed onto two PEN slides. Slides were immediately stained in the following RNase-free, ice-cold solutions (each for 1 min): 70% ethanol, water (with gentle agitation), 1% cresyl violet in 50% ethanol, 70% ethanol, 100% ethanol (with gentle agitation), 100% ethanol (with gentle agitation). Slides were dabbed onto tissue paper to remove excess ethanol, air-dried for 1 min and taken for immediate microdissection (Zeiss PALM Microbeam). Cells were cut at $\times 40$ magnification, keeping laser power to a minimum. Motor neurons were identified by location and diameter $> 30\ \mu\text{m}$. Approximately 120 cells were captured per mouse into Adhesive Cap 500 tubes (Zeiss). RNA was extracted using the Arcturus PicoPure kit (ThermoFisher). RNA ($1\ \mu\text{l}$) was run on an RNA 6000 Pico chip on an Agilent 2100 Bioanalyzer to evaluate RNA quality. 1 ng of RNA was used as input for cDNA library preparation.

Spinal motor neuron cDNA and library preparation. Library preparation for sequencing on an Illumina HiSeq2500 sequencer was carried out using the SMART-seq v4 Ultra Low Input RNA kit (Clontech) following the manufacturer's instructions. All steps were carried out on ice unless otherwise specified. Reverse transcription, PCR cycles and incubation steps utilized a Bio-Rad T100 Thermal Cycler. Amplification of cDNA by LC PCR used a ten-cycle protocol. After bead purification, cDNA library concentration was measured (High Sensitivity DNA kit, Agilent Technologies).

Sequencing libraries were generated using the Nextera XT DNA Library Prep Kit (Illumina) using 150 pg cDNA as input following the manufacturer's instructions with the following modification. Following library amplification and bead purification, the final fragment size was analyzed and libraries quantified using the Universal KAPA Library Quantification kit (Kapa Biosystems) and a Bio-Rad C100 thermal cycler. An equal amount of cDNA was used to pool up to four samples, which were sequenced in one lane. Sequencing was carried out to a depth of 50 million 100-bp paired-end reads per library.

Frontal cortex RNA-seq library preparation. Only RNA samples with RIN > 8 were used for sequencing. Libraries were prepared using the TruSeq Stranded mRNA kit (Illumina) following the manufacturer's low sample protocol with the following modification. RNA fragmentation time was reduced to 3 min at 94°C to increase median insert length. Final libraries were analyzed, quantified and sequenced as above.

Bioinformatics pipeline and statistics. FastQ files were trimmed with Trim Galore v0.4.3 using default settings then aligned against the mouse GRCh38 genome assembly with hisat2 v2.0.5 using options `--no-mixed` and `--no-discardant`. Mapped positions with MAPQ values of < 20 were discarded.

Gene expression was quantified using the RNA-Seq quantification pipeline in SeqMonk v1.37.0 in opposing-strand-specific (frontal cortex) or unstranded (motor neuron) library mode using gene models from Ensembl v67. For count based statistics, raw read counts over exons in each gene were used. For visualization and other statistics, log₂ RPM (reads per million reads of library) expression values were used.

Differentially expressed genes were selected using pairwise comparisons with DESeq2 with a cut-off of $P < 0.05$ following multiple testing correction.

Differential splice junction usage was detected by quantifying the raw observation counts for each unique splice donor/acceptor combination in all samples. Initial candidates were selected using DESeq2 with a cut-off of $P < 0.05$ following multiple testing correction. To focus on splicing specific events, hits were filtered to retain junctions whose expression change was > 1.5 fold different from the overall expression change for the gene from which they derived, or which showed a significant (logistic regression $P < 0.05$ after multiple testing correction) change in observation to another junction with the same start or end position.

A secondary intensity filter akin to a dynamic fold-change filter was applied to DESeq2 hits. DESeq2 comparisons were between wild-type and TDP43^{Q331K/Q331K} mice or between MB+ and MB- mice. Significant expression and splicing changes between wild-type and TDP43^{Q331K/Q331K} were used to generate hierarchical cluster plots including TDP43^{Q331K/+} mice to identify patterns of changes across replicates.

Significant expression and splicing changes between MB+ and MB- mice were used to generate hierarchical cluster plots including wild-type mice.

Gene Ontology and KEGG enrichment analysis. The Database for Annotation, Visualization and Integrated Discovery (DAVID) v6.8 was used for functional annotation of gene expression data in addition to the Functional Enrichment Analysis tool (FunRich v3.0) (available at <http://funrich.org/>). Gene Ontology biological process and KEGG pathway enrichment analysis was conducted using DAVID and FunRich with a threshold Benjamini-corrected $P \leq 0.05$.

Spinal cord RNA extraction for qPCR. Tissues were briefly washed in ice-cold PBS to remove mounting medium and homogenized, and RNA was extracted as described above for frontal cortices and hippocampi.

Quantitative PCR. RNA (500 ng) was reverse transcribed (QuantiTect Reverse transcription kit, Qiagen) and the output volume of 20 μl diluted tenfold in nuclease free water (Promega). Real-time PCR was performed using Brilliant-III Ultra-Fast SYBR (Agilent Technologies) on a Bio-Rad CFX96 instrument with cycle conditions based on Agilent's quick reference guide (publication number 5990-3057, Agilent Technologies). Reaction specificity was confirmed by melt curve analysis and normalized expression ($\Delta\Delta\text{Cq}$) calculated using CFX Manager software 3.1 with at least four reference genes. For qPCR primer sequence, see Supplementary Table 6. Reference genes used were *Ywhaz*, *Pgk1*, *Gapdh* and *Hprt1*. KICqStart SYBR Green primers for these reference genes were purchased from Sigma-Aldrich, in addition to those for *Tardbp*.

Statistical analyses. Statistical analyses were conducted using Prism 6.05 (GraphPad). Graphs were plotted using GraphPad or Python. Use of parametric tests required data to be sampled from a Gaussian distribution. Homogeneity of variance between experimental groups was confirmed by the Browne-Forsythe test for ANOVA and *F* test for unpaired *t*-tests. For comparisons between genotypes or experimental groups, two-tailed, unpaired *t*-tests or one-way ANOVA were used when comparing two or three groups, respectively. Multiple comparisons by ANOVA were corrected using the Holm-Sidak test. Where the assumptions of one-way ANOVA were violated, the non-parametric Kruskal-Wallis test was performed followed by Dunn's multiple comparison test. All statistical comparisons are based on biological replicates unless stated otherwise. Where technical replication of experiments occurs, this is highlighted in the respective method.

Analyses of Rotarod performance, weights and food intake utilized repeated measures two-way ANOVA. Mice lacking measurements at any time point were excluded from analyses. Multiple comparisons by two-way ANOVA were corrected using the Holm-Sidak test.

TDP-43 fluorescence in the nuclear and cytoplasmic compartments of parvalbumin positive cells and cell counts in multiple regions of the cortex were compared using multiple *t*-tests. Multiple comparisons were corrected using the Holm-Sidak test ($\alpha = 5\%$) without assuming consistent s.d.

Statistical analysis: ACBM. The ACBM system characterized each behavior for every frame of recording and quantified the amount of time the mouse was performing a given behavior for each hour (0–23). These data were averaged across 5 d of recording within each animal and then subject to statistical comparison for within-day and between-group analyses.

Statistical analysis to compare the average time spent performing a given behavior between TDP43^{Q331K/Q331K} and wild-type mice was conducted using repeated measures two-way ANOVA, in which the between-subjects variable was genotype and the within-subjects variable was circadian hour (0–23). We report main effects of genotype and genotype \times circadian hour interactions. All statistics were calculated using IBM SPSS Statistics 24, $\alpha = 0.05$. For additional statistical information, see Supplementary Table 7.

Statistical analyses: touchscreen. Data analyses for the touchscreen were conducted using R version 3.3.1. Mixed-effects models were used to identify the main effects of genotype or task conditions (i.e., stimulus duration in 5-CSRTT or delay in object recognition task) and interactions between these factors. Between-genotype differences in sessions to criteria, FR and PR outcomes were analyzed by one-way ANOVA with Holm-Sidak post hoc test.

Randomization. The order and genotype of animals and samples tested was randomized by one operator before subsequent experimental studies were conducted by a second investigator.

Life Sciences Reporting Summary. A Life Sciences Reporting Summary is available online.

Data availability. The authors will make all data available to readers upon reasonable request. RNA-seq data have been deposited and are available at [GSE99354](https://www.ncbi.nlm.nih.gov/geo/).

References

51. Zhu, L. J., Holmes, B. R., Aronin, N. & Brodsky, M. H. CRISPRseek: a Bioconductor package to identify target-specific guide RNAs for CRISPR-Cas9 genome-editing systems. *PLoS One* **9**, e108424 (2014).
52. Heath, C. J., Bussey, T. J. & Saksida, L. M. Motivational assessment of mice using the touchscreen operant testing system: effects of dopaminergic drugs. *Psychopharmacology (Berl.)* **232**, 4043–4057 (2015).
53. Romberg, C. et al. Depletion of perineuronal nets enhances recognition memory and long-term depression in the perirhinal cortex. *J. Neurosci.* **33**, 7057–7065 (2013).
54. Wu, L. S., Cheng, W. C. & Shen, C. K. Targeted depletion of TDP-43 expression in the spinal cord motor neurons leads to the development of amyotrophic lateral sclerosis-like phenotypes in mice. *J. Biol. Chem.* **287**, 27335–27344 (2012).
55. Baghirova, S., Hughes, B. G., Hendzel, M. J. & Schulz, R. Sequential fractionation and isolation of subcellular proteins from tissue or cultured cells. *MethodsX* **2**, 440–445 (2015).
56. Kalmar, B., Blanco, G. & Greensmith, L. Determination of muscle fiber type in rodents. *Curr. Protoc. Mouse Biol.* **2**, 231–243 (2012).

Life Sciences Reporting Summary

Nature Research wishes to improve the reproducibility of the work that we publish. This form is intended for publication with all accepted life science papers and provides structure for consistency and transparency in reporting. Every life science submission will use this form; some list items might not apply to an individual manuscript, but all fields must be completed for clarity.

For further information on the points included in this form, see [Reporting Life Sciences Research](#). For further information on Nature Research policies, including our [data availability policy](#), see [Authors & Referees](#) and the [Editorial Policy Checklist](#).

Please do not complete any field with "not applicable" or n/a. Refer to the help text for what text to use if an item is not relevant to your study. [For final submission](#): please carefully check your responses for accuracy; you will not be able to make changes later.

▶ Experimental design

1. Sample size

Describe how sample size was determined.

Refer to online methods: mouse breeding and maintenance:
To calculate numbers of animals needed for the behavioural studies, power calculations were based on historical rotarod and touchscreen data of wild-type mice studied in the Coleman and Bussey labs respectively. This indicated required group sizes of 15 animals per genotype to pick up a ~20% difference in performance between mutant and wild-type mice.

2. Data exclusions

Describe any data exclusions.

Refer to online methods: mouse breeding and maintenance:
Animals were only excluded from any given analysis if specified in the following methods.
Touchscreen studies:
Animals that had not reached the criterion (> 80% accuracy, < 20% omission in two consecutive sessions in baseline training before entering the probe test, N = 1 in the first probe test) or whose body weights were below 80% of free-feeding weight (N = 1 in the first, and N = 1 in the second probe test) were excluded based on these pre established criteria.
Rotarod:
An individual mouse recording was excluded if it fell off the rod while moving backwards, accidentally slipped or jumped off at slow speed.
RNAseq bioinformatics pipeline:
FastQ files were trimmed with trim galore v0.4.3 using default settings then aligned against the mouse GRCm38 genome assembly using hisat2 v2.0.5 using options --no-mixed and --no-discordant. Mapped positions with MAPQ values of <20 were discarded. This is a pre-designated score for the alignment of reads to a reference genome. The threshold set corresponds to a 1% chance that a read is falsely aligned.

3. Replication

Describe the measures taken to verify the reproducibility of the experimental findings.

Refer to online methods: Statistical analysis:
All statistical comparisons are based on biological replicates unless stated. Where technical replication of experiments occurs, this is highlighted in the respective method.
All data points represent independently collected biological replicates unless specifically identified.
All attempts at replication have been successful.

4. Randomization

Describe how samples/organisms/participants were allocated into experimental groups.

Refer to online methods (ransomisation):
For behavioral studies, the order and genotype of animals and samples tested were randomized by one operator before subsequent experimental studies were conducted by a second investigator.
Animals were age and sex matched for all studies unless stated otherwise and experimental groups were tested at comparable times under common experimental conditions.

5. Blinding

Describe whether the investigators were blinded to group allocation during data collection and/or analysis.

Refer to online methods:
All cognitive testing:
Genotypes of animals were blind to investigators during neurocognitive testing.

Rotarod:

All testing was conducted by operators who were blind to genotype and in a randomised order.

Immunostaining, motor neuron quantification & cellular quantification in brain:
Data analysis using ImageJ 1.15j and imaging was carried out blind to mouse genotype.

Western blot band intensity quantification:

Quantification was carried out by a user blind to the genotype of each lane.

NMJ innervation:

Quantification was carried out by a user blind to the genotype

Note: all in vivo studies must report how sample size was determined and whether blinding and randomization were used.

6. Statistical parameters

For all figures and tables that use statistical methods, confirm that the following items are present in relevant figure legends (or in the Methods section if additional space is needed).

- | | |
|-----|-----------|
| n/a | Confirmed |
|-----|-----------|
- The exact sample size (*n*) for each experimental group/condition, given as a discrete number and unit of measurement (animals, litters, cultures, etc.)
 - A description of how samples were collected, noting whether measurements were taken from distinct samples or whether the same sample was measured repeatedly
 - A statement indicating how many times each experiment was replicated
 - The statistical test(s) used and whether they are one- or two-sided
Only common tests should be described solely by name; describe more complex techniques in the Methods section.
 - A description of any assumptions or corrections, such as an adjustment for multiple comparisons
 - Test values indicating whether an effect is present
Provide confidence intervals or give results of significance tests (e.g. P values) as exact values whenever appropriate and with effect sizes noted.
 - A clear description of statistics including central tendency (e.g. median, mean) and variation (e.g. standard deviation, interquartile range)
 - Clearly defined error bars in all relevant figure captions (with explicit mention of central tendency and variation)

See the web collection on [statistics for biologists](#) for further resources and guidance.

► Software

Policy information about [availability of computer code](#)

7. Software

Describe the software used to analyze the data in this study.

to online methods:

Crispr:

Off-targets were predicted using CRISPRseek.

ACBM:

Cages were monitored with a Firefly MV 0.3 MP Mono FireWire 1394a (Micron MT9V022) at 30 frames/s.

The system used for ACBM was modified from that previously described and was re-implemented in Python and NVIDIA's CUDNN to speed video analysis subroutines. All video analyses were conducted using the Brown University high-performance computer cluster. All statistics were calculated using IBM SPSS Statistics 24, alpha = 0.05.

Touchscreens:

Standard mouse Bussey-Saksida touchscreen chambers were used (Campden Instruments Ltd.)

Data analyses for touchscreen and object recognition tasks were conducted using R version 3.3.1.

Immunofluorescence quantification and histology:

Image stitching was completed using NIS-Elements software.

Data analysis using ImageJ 1.15j

Western blotting and NMJ innervation:

Western blot band intensities were quantified using Fiji (ImageJ; Version 2.0.0-rc-54/1.51h; Build: 26f53ffab) using the programs gel analysis menu option in 8-bit greyscale.

Bioinformatics pipelines:

FastQ files were trimmed with trim galore v0.4.3 using default settings then aligned against the mouse GRCm38 genome assembly using hisat2 v2.0.5 using options --no-mixed and --no-discordant. Mapped positions with MAPQ values of <20 were discarded. Gene expression was quantitated using the RNA-Seq quantitation pipeline in SeqMonk v1.37.0

Differentially expressed genes were selected using pairwise comparisons with DESeq2

GO and KEGG enrichment:

The Database for Annotation, Visualization and Integrated Discovery (DAVID) v6.8 was used for functional annotation of gene expression data in combination with the Functional Enrichment Analysis tool (FunRich v3.0).

Quantitative PCR:

Reaction specificity was confirmed by melt curve analysis and normalised expression ($\Delta\Delta Cq$) calculated using CFX Manager software 3.1

Statistical analysis:

Statistical analyses were conducted using Prism 6.05 (GraphPad). Graphs were plotted using Graphpad or Python.

For manuscripts utilizing custom algorithms or software that are central to the paper but not yet described in the published literature, software must be made available to editors and reviewers upon request. We strongly encourage code deposition in a community repository (e.g. GitHub). *Nature Methods* [guidance for providing algorithms and software for publication](#) provides further information on this topic.

► Materials and reagents

Policy information about [availability of materials](#)

8. Materials availability

Indicate whether there are restrictions on availability of unique materials or if these materials are only available for distribution by a third party.

No unique materials used

9. Antibodies

Describe the antibodies used and how they were validated for use in the system under study (i.e. assay and species).

Refer to methods section for primary antibodies used for immunofluorescence and western blotting.

All antibodies have their respective source company and reference code displayed along with the dilution factor applied.

All antibodies are validated for the applications used within this manuscript and this information is available on the manufacturers publicly available datasheets

In summary:

- 1) ab41881, rabbit to TDP-43 is validated in mouse for immunohistochemistry (IHC) & Western blot (WB)
- 2) ab4680, chicken to TDP-43 is validated in mouse for IHC
- 3) ab11427, rabbit to Parvalbumin is validated in mouse for IHC
- 4) ab5392, chicken to MAP2 is validated in mouse for IHC
- 5) A0024, rabbit to Tau is validated in mouse for IHC
- 6) ab104224, mouse to NeuN is validated in mouse for IHC
- 7) PA5-36922, rabbit to AOX1 is validated in mouse for IHC
- 8) ab8049, mouse to Synaptophysin is validated in mouse for IHC
- 9) T2200, rabbit to β III tubulin is validated in mouse for IHC
- 10) ab41684, rabbit to Cyclophilin is validated in mouse for WB
- 11) mab414, mouse to nucleoporin is validated in mouse for WB

10. Eukaryotic cell lines

a. State the source of each eukaryotic cell line used.

No cell lines used

b. Describe the method of cell line authentication used.

No cell lines used

c. Report whether the cell lines were tested for mycoplasma contamination.

No cell lines used

d. If any of the cell lines used are listed in the database of commonly misidentified cell lines maintained by [ICLAC](#), provide a scientific rationale for their use.

No cell lines used

► Animals and human research participants

Policy information about [studies involving animals](#); when reporting animal research, follow the [ARRIVE guidelines](#)

11. Description of research animals

Provide all relevant details on animals and/or animal-derived materials used in the study.

Refer to online methods: mouse breeding and maintenance:

Mouse line #52 was expanded and used for subsequent studies. This animal was outcrossed with wild-type C57Bl/6J mice through to the F3 generation. Three F3 male sibling mice were bred to wild-type C57Bl/6J mice to generate multiple male and female F4 TDP-43Q331K/+ mutant mice. Multiple breeding pairs of TDP-43Q331K/+ male and female F4 mice were set up. 100 mice of each sex were bred, at which point, due to the non-Mendelian pattern of genotypes in males only, a further 100 male animals only were bred, biopsied and genotyped to confirm the non-Mendelian breeding ratio.

All USA procedures were approved by the Brown University Animal Care and Use Committee.

All UK experiments were conducted in accordance with the United Kingdom Animals (Scientific Procedures) Act (1986) and the United Kingdom Animals (Scientific Procedures) Act (1986) Amendment Regulations 2012.

For the majority of studies male mice were used. Where experiments included female animals, this is stated in the specific methodology or relevant figure legend. Animals were housed in cages of up to five animals under a 12 hr light/dark cycle (lights on at 7:00am) unless stated.

Animals cohorts underwent testing at a variety of ages as detailed in specific methods and figure legends. The oldest animals used were aged to 23 months.

Policy information about [studies involving human research participants](#)

12. Description of human research participants

Describe the covariate-relevant population characteristics of the human research participants.

No participants